UNIVERSIDAD DE
GUANAJUATO

"Computational Study of Phage Adsorption Dynamics on Cell Membranes"

A thesis submitted for the degree of
Master in Physics

Isael Aaron Segoviano Caudillo

Supervisor:
Prof. Francisco Alarcón Oseguera

Universidad de Guanajuato - Campus León
División de Ciencias e Ingenierías

GUANAJUATO, MÉXICO. Junio 2025

Acknowledgements

Quiero expresar mi más sincero agradecimiento a mi asesor, Francisco Alarcón, por su orientación, apoyo y valiosas discusiones a lo largo del desarrollo de este trabajo. Asimismo, agradezco los recursos computacionales proporcionados por MesoSimLab, los cuales fueron fundamentales para la realización de las simulaciones presentadas en esta tesis. También agradezco al proyecto 142/2024 de la Convocatoria Institucional de Investigación Científica de la Universidad de Guanajuato.

Este trabajo fue posible gracias al acceso a tiempo de cómputo otorgado por las siguientes instituciones: a) Laboratorio Nacional de Cómputo de Alto Desempeño (LANCAD) y la Secretaría de Ciencia, Humanidades, Tecnología e Innovación (SECIHTI) en el supercomputador MIZTLI en DGTI UNAM en las convocatorias 2024 y 2025 b) Laboratorio de Supercómputo del Bajío (Lab-SB) CIMAT, a través de las convocatorias 2024 y 2025 "Supercómputo como motor de colaboraciones academia–industria", en conjunto con el Instituto de Innovación, Ciencia y Emprendimiento para la Competitividad para el Estado de Guanajuato (IDEA GTO) y SECIHTI.

Agradezco también a SECIHTI, por la beca otorgada que hizo posible la realización de este trabajo.

Extiendo mi agradecimiento a los miembros de mi comité de seguimiento académico por su apoyo, orientación y observaciones constructivas durante el desarrollo de esta investigación. Finalmente, agradezco a todos los integrantes de MesoSimLab, ya que cada uno de ellos contribuyó en al menos una ocasión al avance de este trabajo.

"Wake me… when you need me."

— Master Chief

Abstract

The motivation of this work originated from the interest in understanding viral adsorption phenomena from a physical perspective, particularly in systems involving anisotropic particles such as bacteriophages. When suspended in a fluid, bacteriophages interact with bacterial surfaces through a combination of hydrodynamic effects, steric constraints, and anisotropic surface affinities. Therefore, their adsorption and alignment on cellular membranes are governed not only by biochemical interactions but also by fluid-mediated transport and orientation processes.

To capture these features, we developed a coarse-grained model composed of anisotropic dimers embedded in a dissipative fluid. The dimers represent elongated viral particles, where anisotropy is introduced through interaction asymmetry between the two components. Bacterial surfaces were represented by granular walls, which allow control of physical characteristics such as roughness and affinity distribution. The construction of the model is intentionally general: although motivated by phage–bacteria interactions, it can be tuned to reproduce other physical systems that share similar geometric constraints, adsorption mechanisms, or anisotropic interactions.

Dissipative Particle Dynamics (DPD) was selected as the simulation method due to its ability to simultaneously reproduce hydrodynamic behavior, excluded-volume interactions, and mesoscale thermal fluctuations. Within this framework, we performed systematic studies on the effects of wall morphology, surface affinity, hydrophobicity on dimer adsorption and an analysis of the orientational behavior of the dimers was conducted, revealing how hydrodynamic conditions and heterogeneous surface affinities influence the system.

Contents

1 Introduction **6**

1.1 Bacteriohages 6
1.2 Infection 8
1.3 Modeling background 8
1.4 Contribution 9
1.5 Conclusions 9

2 Theory **11**

2.1 Molecular Simulations 11
2.2 Mesoscopic Methods 12
2.3 Dissipative Particle Dynamics 14
2.4 High-Performance Computing 16
2.5 Conclusions 18

3 Model and Characterization Tools **19**

3.1 Phage Model 19
3.2 Wall Model 21
3.3 Tools 22
3.3.1 Mean Square Displacement 23
3.3.2 Orientational Order Parameters 23
3.3.3 Adsorption Isotherms 24
3.4 Conclusions 25

4 Benchmarking **26**
4.1 DPD in LAMMPS 26
4.2 Explicit Walls in LAMMPS 30
4.3 Fluid Flow Modeling 38
4.3.1 Navier-Stokes equations 38
4.3.2 Couette Flow 39
4.3.3 Poiseuille Flow 42

5 Static Case **46**
5.1 Abstract 46
5.2 Simulations Details 47
5.3 Hydrophobic Interaction of the Walls 47
5.4 Heterogeneus Walls 56
5.5 Conclusions 71

6 Dynamic Case **73**
6.1 Abstract 73
6.2 Non-Slip Conditions 73
6.3 Poiseuille With Non-Slip Conditions 74
6.4 Poiseuille With Slip Conditions 76
6.5 Couette With Non-Slip Conditions 77

7 Conclusions and Perspectives **79**

Bibliography **81**

8 Appendix **87**
8.1 Adsorption in function of affinity zone 87

Chapter 1

Introduction

In this chapter, we will present the motivation behind this project and outline the key concepts necessary for understanding it. Before delving into the physics, we begin by discussing the biological relevance of bacteriophages and their nature. We then address the mechanisms by which viruses, particularly bacteriophages, infect bacteria, and explain why this phenomenon is central to our study. Following this, we describe the modeling framework used to approach the physical aspects of the problem, including the relevant theoretical background. We review previous studies and the current state of the art, highlighting the existing gaps in knowledge. Our specific contributions to the understanding of this biophysical problem are also introduced. Finally, we conclude with a summary of the chapter and outline the key ideas that will guide the rest of the work.

1.1 Bacteriohages

The bacteriophages (phages) are viruses that infect bacteria. It was discovered at 1915 by the physician Frederick Twort and the microbiologist Felix d'Herelle [1, 2]. The phages are a biological entity very relevant for the science. Thanks to its behaviour, they have a lot of po-

tential. They are the most abundant biological entities on Earth [3]. At this moment, we host around trillion of phages in intestinal flora.

The bacteroiphage was widely studied but, it is estimated that there are tens of millions of phage species in nature [4]. At GenBank have listed around 1500 phage genomes and the most of them are not been studied. This means that the bacteriophages are very diverse, because they might have different size of capsid, different lenght of tail, some even have no tail. So much that the RNA cointained in each phage is very diverse too.

The bacteriophage plays an important role for nature, its behavior as bacteria killer become relevant because with that, the phage controls the bacteria population at enviroments that if they were not there, there would be unpleasant consequences like the bacteria population at the ocean [5]. Many of them infect different types of bacterias like Escherichia coli, Salmonella, Straphylococcus, etc.

The human is always learning of nature to develop new technologies and solve current problems. One of the current and most important problem in the healt industry is the antibiotic-resistant bacteria (superbacteria). Due to the improper use of antibiotics therefore, the World Health Organization (WHO) declared that the superbacteria will be a big problem for the human health [6]. Therefore, it becomes a relevant subject to study, Many studies have proven that the phages are a viable solution for this problem [7], in nature, the phages help to controls the bacteria populations even in our microbiota. We can take advantage of this property and use bacteriophages as a tool to combat bacteria responsible for severe diseasess or antibiotic-resistant infections.

1.2 Infection

The morphologic structure of bacteriophage will be discussed with detail in section 3.1. For now, we will comment quickly that phages are conformed (generally) by a icosahedral capsid, a cylinder, a baseplate and long-tail fibers attached to the baseplate. Phages are viruses and they do not have self motility, its movement is due to thermal fluctuations [8] and another physical interactions like electrostatic forces [9].

With this kind of movement, they are able of move towards the surface of some bacteria. They can conect its long-tail fibers to proteins on the surface and looking for a region to infect. Once phage finds the right place, it proceeds to infect, contracting its cylinder to use it like a syringe to inject its RNA into a bacterium and uses it as a replicant [10].

Our interest does not lie in modeling the full infection process, but specifically in the mesoscale regime during which the phage approaches the bacterial cell wall in search of an infection site.

1.3 Modeling background

Studies have been conducted on the encounter rates between phages and bacteria, such as in ref. [8], where phages are modeled using Brownian dynamics and bacteria are treated as active particles. As noted in ref. [8], it is reported that the properties of the surrounding fluid affect the diffusion of the phage. A similar study has been done in our research team focused in collective behaviors [11]. Additionally, studies on mixtures of active and passive particles have been carried out [12], which are particularly relevant to this project due to the similarity with such systems. Moreover, within the same research group, studies have been performed with mixtures of brownian particles and active

particles, where diffusion was analyzed by varying the concentrations of both Brownian and active particles [13].

The use of computational simulations is particularly relevant due to their great potential for reproducing these systems. Much of the current understanding of phages has been achieved thanks to simulations, as is also the case for the infection processes such as ref. [14].

1.4 Contribution

In the aforementioned studies, the anisotropy of the bacteriophage is not taken into account. It is typically modeled as a single particle. However, it is evident that infection occurs via the tail structure. Therefore, the orientation with which the phage approaches the cell membrane may influence the infection dynamics.

In this project, we develop a DPD (Dissipative Particle Dynamics) model that explicitly accounts for this anisotropy. In contrast to previous studies, our approach focuses specifically on the timescale in which the phage is searching for attachment to the bacterium in order to initiate infection.

The motivation for using DPD in this work lies in one of our key contributions: analyzing the hydrodynamic interactions in the system and evaluating their influence on the adsorption dynamics.

1.5 Conclusions

In this chapter, we introduce the motivation given by bacteriophage infection, emphasize the relevance of their anisotropy, and discuss some

of the previous work carried out within our research group. As well as our contributions to the current understanding of these phenomena.. It is important to emphasize that, despite the specific motivation of this work, the developed system is general. It consists of particles interacting with each other through interaction potentials. Therefore, the model can be adapted to other physical systems, such as surfactants, Janus colloids, etc.

Chapter 2

Theory

During the last century the scientists have been developed simulations methods to simulate the fluid as we said before. In this section we are going to discuss about the methods used in this project. For example how do we integrate the equations of motion, how do we model real system. In particular we will talk in section 2.3 about the model of Dissipative Particle Dynamis with more details. Finally, to be more specific, we discuss how do we compute the equations of motion of this model with the package LAMMPS in C++.

2.1 Molecular Simulations

In the reference [15] says that if we could have phisicists in a closed room, without contact to the exterior, the unique contact is the four walls of concrete, with sufficient time they could discover many incognits about the vanguard phisics like, quantum physics, electrodynamics, etc. However one thing that they could not discover, is the liquid phase. The fluids has a enigmatic behaviour and is very difficult to describe its nature. Boltzman [16, 17] says that if we have the exact position of each particle that conforms the fluid, we could describe the movement resolving the equations of motion. However it is unfeasible, given that

the number of particles involved would be on the order of Avogadro's number. Therefore, through the history the phisicists have developed methods with the help of the computers, making codes to resolve the motion and the case of the ergodic hipothesis.

In some cases is very difficult or impossible to get a exact solution for a problem, for example a 3-body interaction. If we want to simulate physical systems like a fluid, is necessary to use many more particles therefore. Introducing an additional component to the fluid, such as dimers, would render an analytical solution for this system unfeasible at the relevant scales. Using computing simulations we can modelate the system with a certain precision and statistical error.

The computing simulations can be used as a way to prove a theory, i.e. a computer experiment, comparing the results of the simulation and the analytical solutions of the theory. Another way to use the computing simulations is comparing the results of simulations with the real experimental data, in the simulation we can to define the pair potential for the particles, and we can estimate the interaction potential for the real case. With all that said, we can put the computing simulations at the interface between theory and experiments.

2.2 Mesoscopic Methods

As we know, something important in Physics are the scales, the scales make a difference between various areas of Physics, like quantum, nuclear, atomic, molecular and even cosmic physics. One particular scale is the mesoscopic scale, this scale help us to resolve phenomena beyond the atomistic resolution, talking in the context of the International System of Units, around the nanometers.

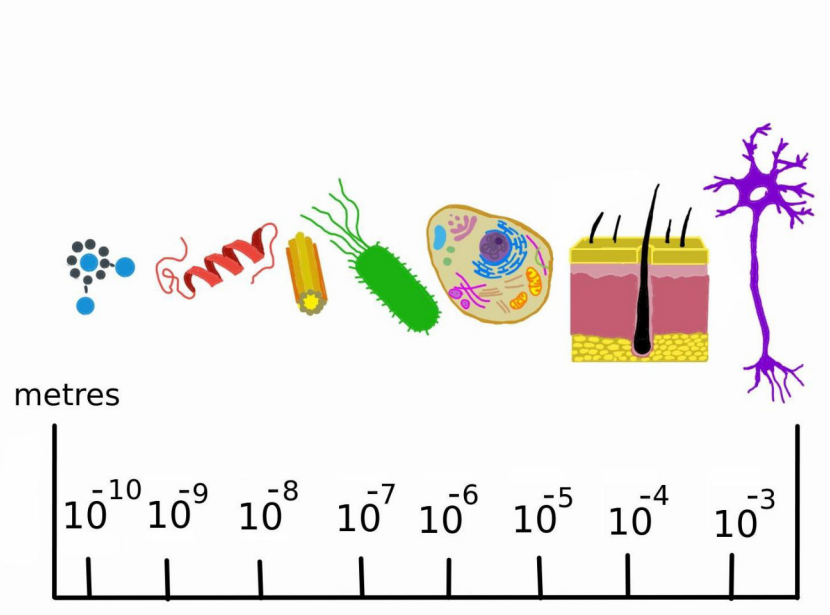

Figure 2.1: Physical systems together with their corresponding spatial scales, including bacterias, chromosomes, proteins, etc.

The mesoscopic scale is defined in space and time. In the space region is defined from 10-10^4 nm or, 10^{-8}-10^{-5} m as you can see in figure 2.1. With respect to timescale, the mesoscale is defined from 1-10^6 ns [18].

We can study physical systems like fluids as we saw in the past section, we can use continuum theories as Navier-Stokes to describe from a macroscopic approach. However, most of the time there are not analytical solutions for this approach. The most common alternative is to see the problem with an atomic approach to solve the dynamics for each particle.

To resolve a system within atomistic scale usually works, but it cost a lot of computing resources, being very difficult to study the system and sometimes imposible due to the computing time. At this moment

the use of mesoscopic methods becomes relevant, we can use particles that represents a segment of a field (like a fluid) and it cost less computing resources but, using a discrete method.

With the statistical physics we can study the system as interacting particles, compute averages over the ensembles and recover the macroscopic behaviour as we will see in the next section with the Dissipative Particle Dynamics method.

2.3 Dissipative Particle Dynamics

In the world of the computational simulations there are many different methods to simulate complex fluids, one of these is the dissipative particle dynamics (DPD). This method consists in beads that each DPD bead represents a segment of the fluid, where the interaction is pairwise, mediated by three types of forces. The dynamics are given by the Newton equation

$$\mathbf{F}_i = m_i \frac{d^2\mathbf{r}_i}{dt^2}. \tag{2.1}$$

The net force on a i-th particle is given by the sum of the three types of forces produced by the rest of particles in a cutoff radius r_c as follow.

$$\mathbf{F}_i(\mathbf{r}) = \sum_{i \neq j} \left(\mathbf{F}^C_{ij} + \mathbf{F}^D_{ij} + \mathbf{F}^R_{ij} \right). \tag{2.2}$$

The three forces are the following

$$\begin{aligned} \mathbf{F}^C_{ij} &= a_{ij}\omega^C(r_{ij})\hat{\mathbf{r}}_{ij}, \\ \mathbf{F}^D_{ij} &= -\gamma\omega^D(r_{ij})(\hat{\mathbf{r}}_{ij} \cdot \mathbf{v}_{ij})\hat{\mathbf{r}}_{ij}, \\ \mathbf{F}^R_{ij} &= \sigma\omega^R(r_{ij})\xi_{ij}\hat{\mathbf{r}}_{ij}, \end{aligned} \tag{2.3}$$

where they are a conservative force $\mathbf{F}^C_{ij}$, a dissipative force $\mathbf{F}^D_{ij}$ and a random force $\mathbf{F}^R_{ij}$ due to the thermal effects. Where $\mathbf{r}_{ij} = \mathbf{r}_i - \mathbf{r}_j$. a_{ij} is

the amplitude of the conservatice force, when $\mathbf{r}_i = \mathbf{r}_j$ the value of the conservative force is equal to a_{ij} being the maximum. The term γ is the friction coefficient and σ the amplitude of the noise.

Also in the equations 2.3, $\omega^C(r_{ij})$, $\omega^D(r_{ij})$, $\omega^R(r_{ij})$ are the weight functions with the following relations

$$\omega^C(r_{ij}) = \begin{cases} 1 - \dfrac{r_{ij}}{r_c} & r_{ij} < r_c \\ 0 & r_{ij} \geq r_c \end{cases},$$

$$\omega^D(r_{ij}) = \left[\omega^R(r_{ij})\right]^2 = \begin{cases} \left(1 - \dfrac{r_{ij}}{r_c}\right)^2 & r_{ij} < r_c \\ 0 & r_{ij} \geq r_c \end{cases}. \tag{2.4}$$

The term ξ_{ij} is a Gaussian noise, satisfying the following properties

$$\left\langle \xi_{ij}(t) \right\rangle = 0, \tag{2.5}$$

$$\left\langle \xi_{ij}(t)\xi_{kl}(t') \right\rangle = (\delta_{ik}\delta_{jl} + \delta_{il}\delta_{jk})\delta(t - t').$$

With this all considerations, it is possible to get a stochastic differential equation for the i-th particle following the procedure in ref [19].

$$\begin{aligned} m_i \frac{d\mathbf{r}_i^2}{dt^2} dt = & \sum_{j \neq i} a_{ij} \omega^C(r_{ij}) \hat{\mathbf{r}}_{ij} dt \\ & -\gamma \sum_{j \neq i} \omega^D(r_{ij})(\hat{\mathbf{r}}_{ij} \cdot \mathbf{v}_{ij}) \hat{\mathbf{r}}_{ij} dt \\ & +\sigma \sum_{j \neq i} \omega^R(r_{ij}) \hat{\mathbf{r}}_{ij} dW_{ij}, \end{aligned} \tag{2.6}$$

where dW_{ij} is an independent increment of the Wiegner process. Considering the evolution of the probability density $\rho(r, p; t)$ and using Itô's rule, Español and Warren derived the Fokker-Planck equation, it describes the temporal evolution of the distribution function $\rho(r, p; t)$ of

the position and momentum of the particles.

$$\frac{\partial \rho(r,p;t)}{\partial t} = L_C \rho(r,p;t) + L_D \rho(r,p;t), \tag{2.7}$$

where L_C is the Liouville operator of the Hamiltonian system interacting with conservatives forces, L_D is an operator with second derivatives and dissipative and random terms. If the dissipative and random force are turn off, they obtain the Gibbs-Boltzmann distribution in the canonical ensemble. Then, turn on the dissipative and random force. To derive the Navier–Stokes equations, it is necessary to enforce momentum conservation. To satisfy this requirement, Español and Warren concluded that is necessary to choose the following propertie along with 2.4

$$\sigma^2 = 2\gamma K_B T, \tag{2.8}$$

in addition to that the noise being symmetric $\xi_{ij} = \xi_{ji}$ to satisfy that the equilibrium distribution won't move away from the equilibrium Gibbs-Boltzmann distribution when you turn on the dissipation and noise.

2.4 High-Performance Computing

As we seen in the previous section, DPD is a simple model. However, it is necessary to perform computational calculations involving a large number of particles over extended periods of time, which would require a significant amount of computational resources. We opt for using parallel programming to concentrate our efforts to analize and make codes to compute observables and parameters to caracterize the system.

The parallel programing is a paradigm where the proces of a program is not carried out linearly, the task is divided into smaller subtasks, each subtask is carried out simultaneously and indepentently in a different processing unit, therefore it is necessary to use multiple CPU cores.

In our laboratory we use parallel programming on multi-core CPUs using threads, however recently we use communication between multiple processes acrooss different nodes thanks the acces to the supercomputer ”Miztli” from National Laboratory for High-Performance Computing (LANCAD by its acronym in spanish) belonging to UNAM. Additionally, access was granted to the high-performance computing cluster at the Center for Research in Mathematics (CIMAT by its acronym in spanish), providing essential computational resources for the study.

Miztli belongs to the fifth generation of supercomputing at UNAM. Its name means ”big feline” in the native lenguage, Nahuatl. This supercomputer is conformed of 332 servers and a storage system of 750 Terabytes. With a total of 5312 processing cores and a capacity pf 118 Teraflop/s and 16 NVIDIA M2090 GPUs. It has capacity of 23 Terabytes in RAM Memory. It uses RedHat Enterprise Linux as operating system.

It is important to note that a considerable amount of time would be required to parallelize our codes. Therefore we use LAMMPS as tool to carry out our simulations. LAMMPS means Large-Scale Atomic/Molecular Massively Parallel Simulator [20]. It is a classical molecular dynamics code. We use it by its power in soft matter and coarse-grained systems. LAMMPS runs in parallel using message-passing techniques as MPI. Message Passing Interface (MPI) is the most commonly used framework in supercomputing. Within molecular dynamics simulations, each node calculates local forces and communicates the positions of particles at the domain boundaries. LAMMPS is a very complex code, with many different options, modifying each parameter. Moreover,, it included many different potentials.

To use LAMMPS, you need to write an input script to be executed line by line. In [21] you can know the typical structure for a input script:

- Initialization Settings: Dimensions, units, boundary conditions, type of particles, etc.
- System Definitions: Length of the box, masses, initial conditions, etc.
- Simulations settings: Force field for each type of particle.
- Simulation execution: Time steps, iterations, etc.

You cand find in LAMMPS many different packages to use according to your needs. To our project, the most important package is DPD-BASIC, containing the basic tools to use DPD simulations. Additionally, the MOLECULE package was employed, as it enables the construction of larger molecules formed by multiple particles.

2.5 Conclusions

With the previous text we see that the molecular simulations are relevant to study systems with many particles and to recover macroscopic behavior. We can use a mesoscopic method like Dissipative Particle Dynamics to recover the hydrodynamics of the system. We opt for using the LAMMPS code to focus on the calculation of observables.

Chapter 3

Model and Characterization Tools

As we said in section 2.2 the mesoscopic model is very useful in molecular simulations, therefore in this section we describe how do we make the model of the phages and cell membrane using a mesoscopic model and how do we implement to our system. We will also talk about the tools we used to analyze the simulations, calculate observables and caracterize the system.

3.1 Phage Model

There are many different types of bacteriophages, there are phages with a long tail, short tail, even without tail. The tail can be crontractile or non-contractile. Therefore we will generalize the model to a "standard model", the most abundant phage and the most studied is the Bacteriophage T4.

The phage T4 has a icosahedral capsid (head) with 115 *nm*-long and 85 *nm*-wide, the capsid is built mainly of proteins [22]. The capsid has a radial distribution density as you can see in figure 3.1, where the concentration of mass is at the perimeter of the capsid, the concentric layers into the capsid are the folded genomic DNA.

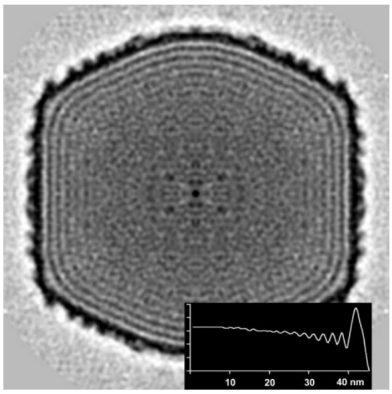

Figure 3.1: Density map of T4 capsid, the high-density regions are darker. As inset plot, the radial distribution density of capsid. Figure extracted from ref. [22].

With respect to the tail, it is conformed by two concetric protein cylinders, the neck, the baseplate and the long-tail fibers. It is a contractile tail with 100 *nm*-long and 21 *nm*-diameter. At the end of cylinders has the baseplate [23].

It has six fibers conected to the baseplate called long-tail fibers. As first step, the phage use this fibers for the attachmente to a bacteria being an adsorption devices [24]. This fibers are 145 *nm*-long and 4 *nm*-diameter [25].

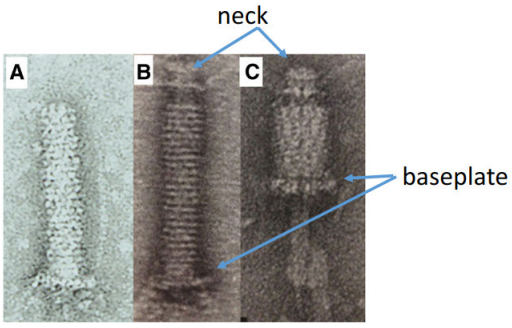

Figure 3.2: a) Extended tail with baseplate. b) Extended tail with baseplate and neck. c) Contracted tail with baseplate and neck. Figure extracted from [26]

With all these considerations we can model the bacteriophage as two

sections. One bead for the capsid, to modify the interactions due to the high mass density and a second bead considering the tail including the base plate and the fibers to modify the interactions due to the contractile tail and the fibers used as adsorption devices. As you can see in figure 3.3

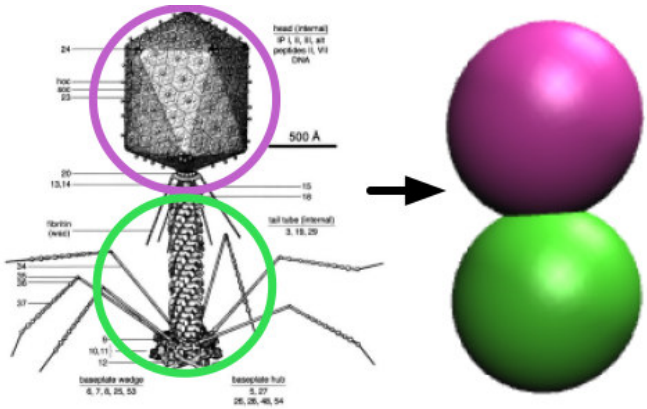

Figure 3.3: Figure of bacteriophage T4 and our DPD model with two beads. Purple bead corresponding to the capsid. Green bead corresponding to tail, baseplate and fibers. Figure taken from ref [10]

The two particles of the dimer are connected by a harmonic bond, where K is the harmonic constant, $\mathbf{r}_h$ and $\mathbf{r}_t$ are the position of the head (purple bead) and the tail (green bead). While l_0 is given by $l_0 = |\mathbf{r}_h - \mathbf{r}_t|^2$. The harmonic force is given by

$$\mathbf{F}(r) = K\left(|\mathbf{r}_h - \mathbf{r}_t| - l_0\right)\frac{\mathbf{r}_h - \mathbf{r}_t}{|\mathbf{r}_h - \mathbf{r}_t|}. \tag{3.1}$$

3.2 Wall Model

As we said previously, the motivation arised by trying to understand the interaction between cell membrane and phages. Then, it is necessary to build a cell membrane, however we are aware that the cell membrane is very complex. Basically, the cell membrane is built with phospholipid

molecules, they are amphiphilic molecules, where the hydrophobic side joins in a bilayer, leaving the hydrophilic side on the outer zone.
This bilayer is the basis for the membrane, as we know, is very complex and it can have inset proteins as you can see in figure 3.4.

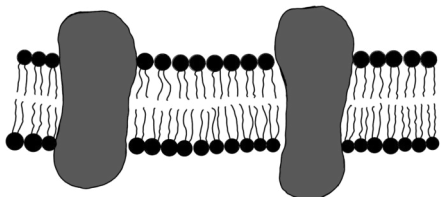

Figure 3.4: Representation of cell membrane where the balls with two chains represent to phospholipids and the large structures represent to proteins in the membrane.

The membrane can have more components like polysaccharides from biofilms, etc. But, we will only consider the proteins. This is because the phage can interact with the cell thanks to the proteins [24]. The size of bacteria is around $1\mu m$, one order of magnitude of difference to the phage [8]. Therefore we will model our cell membrane as a explicit wall, with DPD-beads forming a square lattice, DPD-beads take effectively the rest of components, another class of DPD-beads will be assigned to represent the proteins and other components responsible for producing an effective affinity toward the phage.

Important to remark, we can use an implicit wall, but if we want to add the affinity zones, is more difficult modify the wall potential, therefore, if we use a explicit wall, we easily can use as many types of beads as we want to build a heterogeneus wall.

3.3 Tools

In this subsection we describe the tools used to work with this project, looking for caracterize our system, we were searching what was the

more relevant observable to get information about the system.

3.3.1 Mean Square Displacement

Our first tool to measure is the mean square displacement, this parameter consist in a function of t and is the difference between the position of the i-th particle at time zero and its position at time t, then we compute the mean of all particles as we can see in the following equation

$$MSD = \frac{1}{N} \sum_i |\mathbf{r}_i(t) - \mathbf{r}_i(0)|^2 . \tag{3.2}$$

With this measure we can quantify the mean of displacement of particles from their initial position. As you can see in ref. [27] We can calculate the time correlation function for $r(t)$ at m dimensions and its related transport coefficient D as follow

$$D = \frac{1}{m} \int_0^\infty \langle \dot{\mathbf{r}}_i(t) \dot{\mathbf{r}}_i(0) \rangle dt, \tag{3.3}$$

using integration by parts, considering at large t we can get

$$2tD = \frac{1}{m} \left\langle |\mathbf{r}_i(t) - \mathbf{r}_i(0)|^2 \right\rangle , \tag{3.4}$$

finally we have the relation used to compare our MSD results of simulations and the proportionality to t and the diffusion coefficient.

$$MSD = 2mDt \tag{3.5}$$

3.3.2 Orientational Order Parameters

Another useful measurements in this project are the orientational order parameters. When we have anisotropic particles we can define a vector $\hat{\mathbf{n}}$ associated to the orientation of the particle, like a dipole. As first parameter we have the Polar-Order, that consist in a sum of vectors

of each dipole and we compute the temporal mean. This parameter was used since Born [28] to study the transient states of nematic liquid crystals.

$$O_P = \left\langle \frac{\left|\sum_i^N \hat{\mathbf{n}}_i\right|}{N} \right\rangle_t . \tag{3.6}$$

In this system we have a wall, the interaction between our anisotropic particles and the wall is very important because if the purple bead touch the wall there is not a infection by the phage, it must touch the wall with the green bead to consider the posibility of infection. Then we will consider a orientation with respect to the wall, we call it Wall-Order and it is defined as the following equation

$$O_W = \left\langle \frac{\sum_i^N \hat{\mathbf{n}}_i \cdot \hat{\mathbf{w}}}{N} \right\rangle_t . \tag{3.7}$$

Where $\hat{\mathbf{w}}$ is the normal vector of the wall.

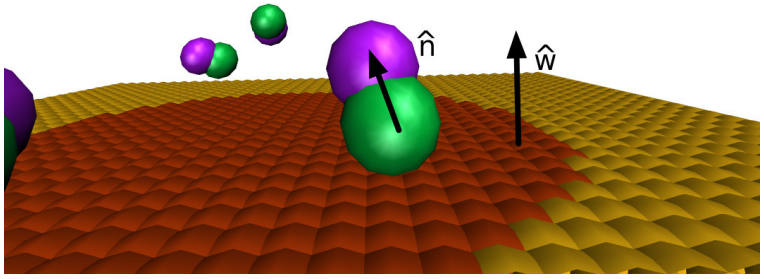

Figure 3.5: Snapshoot of a dimer adsorbed by the wall, the vector $\hat{\mathbf{n}}$ with the direction tail-head and the vector $\hat{\mathbf{w}}$ being orthonormal to the wall.

3.3.3 Adsorption Isotherms

Once the density profile $\rho(y)$ is computed, which consists of a histogram along the y-coordinate using spatial bins and calculating the temporal average, we can obtain the adsorption isotherm using the following

equation:

$$\Gamma(\rho_b) = \int_0^L [\rho(y) - \rho_b]\, dy, \tag{3.8}$$

where ρ_b is the value of the density profile in the bulk and L is the length of the box of simulation. Alternatively, we can define the following absolute adsorption, Γ_{abs}. Both definitions provide complementary insights for the experimental characterization of the adsorption process.

$$\Gamma_{abs}(\rho_b) = \int_0^{\lambda L} \rho(y) dy, \tag{3.9}$$

where λL is the lenght of the gap considering the adsorbed particles. It is important to highlight that we just consider the first layer on the density profile, considering that the rest of layers are consequence of the adsorption of dimers over themself.

3.4 Conclusions

As you saw, the biological systems are very complex and they have many components that we can model. As you know in physics we usually do aproximations, then we can do a first or a second aproximation and see what happens. It is important to emphasize that, we will use a simulation box with a very general structure, therefore it can be applied to another systems with similar features. We know that could be very difficult to understand this specific biological system, therefore we can see this work as a study of fundamental science of a general system of dimers embbeded in a fluid between heterogeneus walls.

Chapter 4

Benchmarking

To ensure that the tools, models, and software packages are working correctly, we have compared with known results of another studies, as benchmarking. Once we can reproduce previous results, we are able to predict phenomena that we are interested on it. We start to modify from this benchmarking the models and to develope more complicate problems.

4.1 DPD in LAMMPS

To test that LAMMPS is working properly, we have used results of ref. [29] as benchmarking. Groot and Warren systematically studied the timestep in DPD simulations to identify the regions of stability and ensure the correct reproduction of thermodynamic properties. They also examined the pressure of the fluid and its relationship with the repulsion parameter a. Furthermore, they investigated the interfacial tension between homopolymer mixtures and the Flory–Huggins model parameter. We will focus only on try to reproduce figure 1, 3 and 4 of their paper.

Using the equation $\sigma^2 = 2\gamma K_B T$ (explained in section 2.3) Groot

and Warren studied the equilibrium of the temperature with different methods, like Euler method and a modified version of the Verlet algorithm [27]. We replicate the figure 1 from [29] with the Verlet method. With a simulation box of size 10x10x10 (with units r_c^3), conservative parameter $a = 25$ and viscosity parameter $\gamma = 4.5$ to have $\sigma = 3$ that is the same system used by Groot and Warren. LAMMPS compute the temperature with the following equation

$$K_B T = \frac{2E_k}{nN - n - N_{DOF}}, \tag{4.1}$$

where E_k is the total kinetic energy of the atoms, n is the dimentionality of the simulation, N is the number of atoms and N_{DOF} is the number of degrees of freedom removed in the simulation [20]. We carried out simulations with the modified Verlet algorithm as follows

$$\begin{aligned} \mathbf{r}_i(t + \Delta t) &= \mathbf{r}_i(t) + \Delta t \mathbf{v}_i(t) + \frac{1}{2}(\Delta t)^2 \mathbf{F}_i(t), \\ \tilde{\mathbf{v}}_i(t + \Delta t) &= \mathbf{v}_i(t) + \lambda \Delta t \mathbf{F}_i(t), \\ \mathbf{F}_i(t + \Delta t) &= \mathbf{F}_i[\mathbf{r}(t + \Delta t), \tilde{\mathbf{v}}(t + \Delta t)], \\ \mathbf{v}_i(t + \Delta t) &= \mathbf{v}_i(t) + \frac{1}{2}\Delta t[\mathbf{F}_i(t) + \mathbf{F}_i(t + \Delta t)]. \end{aligned} \tag{4.2}$$

Where the usual version of Verlet method is recovered for $\lambda = \frac{1}{2}$, this is the value selected for the variable factor λ for the rest of simulations. In this section we study the fluctuation of temperature for different values for λ. Starting the simulation with $K_B T = 1$ we analyzed the variation of the temperature as the simulation runs. The temperature is calculated by $\langle E_k \rangle$ in the long-time limit, and the results are presented in figure 4.1.

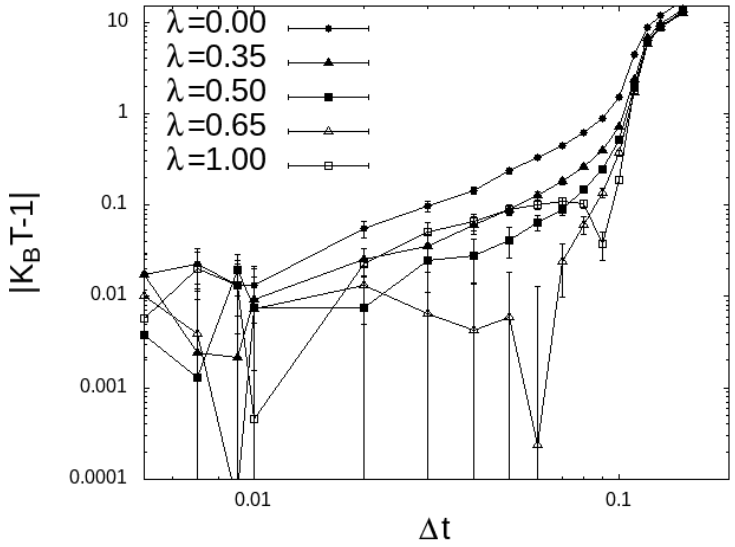

Figure 4.1: $K_BT - 1$ as a function of timestep with $\rho = 4$ and 4 values for λ. For $\lambda = 0.65$, the deviations are on the order of $K_BT - 1$, which makes them appear significantly larger when represented on a logarithmic scale.

In figure 4.1 you can see that up to $\Delta t = 0.4$ the temperature increment is low and acceptable. Obtaining the same results of the paper. Thus, LAMMPS reproduces expected results in terms of integration of equations of motion. It can be seen that for short timesteps, i.e., below $\Delta t = 0.01$, the temperature fluctuations remain unchanged.

Now in the same simulation box and the same DPD parameter we carry out simulations with different densities, where $\rho \in [0.1, 6.0]$. We compute the time average of excess pressure for each ρ and plot $\frac{P-\rho K_BT}{a}$ in figure 4.2 to reproduce the equations of state of DPD as in reference [29].

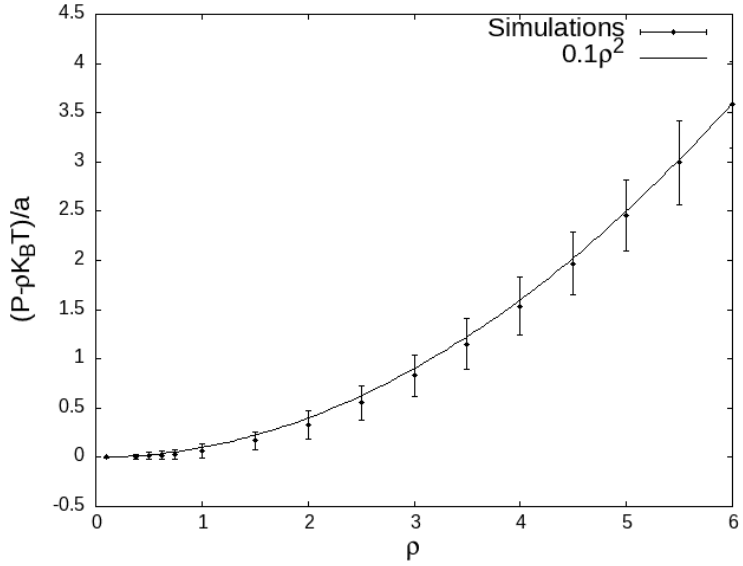

Figure 4.2: Excess pressure as a function of density with a quadratic adjustment.

The pressure is compute as the following equation using the virial theorem

$$P = \rho K_B T + \frac{2\pi}{3}\rho^2 \int_0^1 r f(r) g(r) r^2 dr, \tag{4.3}$$

where we can compute just the equation (4.4) from the figure 4.2. $g(r)$ is the radial distribution function and $f(r)$ is the conservative force of DPD.

$$\frac{2\pi}{3} \int_0^1 r f(r) g(r) r^2 dr = \frac{P - \rho K_B T}{\rho^2} \tag{4.4}$$

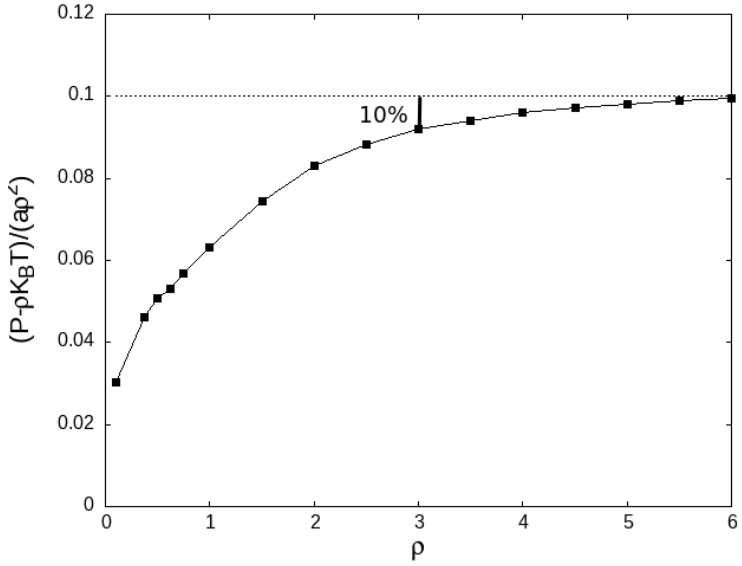

Figure 4.3: Excess pressure as a function of density divided by $a\rho^2$.

Using the numerical results from 4.2 divided by $a\rho^2$ we get the figure 4.3. If we aim to recover the equation of state of DPD, then expression (4.4) must remain constant in order to ensure the proportionality of the integral to the parameter a from (2.3). As a conclusion, we need to use a $\rho > 2$ to obtain a excess pressure proportional to ρ^2 with a maximum error of 10%. Therefore we can use an aproximation as the following equation

$$P = \rho K_B T + \alpha a \rho^2 \tag{4.5}$$

where α is a constant with value $\alpha = 0.101$. As you can see, we obtained a good agreement with Groot and Warren, therefore we can use LAMMPS knowing that it is working well.

4.2 Explicit Walls in LAMMPS

When we are working with bounded systems by walls, we can implement it in two ways. The first is with implicit wall, we can add a force in the system that interact with the particles in the system simulating the

existence of a wall [30]. The second way is with a particle based wall, with this method we add fixed DPD particles that model the wall [31], with a specific arrangement, since they are DPD particles, they interact with the rest of the DPD particles.

The principal differences between both ways is that, with implicit walls we can save calculation time, while with a explicit wall we must calculate each interaction between bulk particle and wall particle. Both wall models have their pros and cons, with a explicit wall we have tuning flexibility, that is to say, we can modify the wall arrangement, the distance between the wall particles and the most important for this work, explicit walls allow us to model heterogeneus walls easily.

In this project we opted for using a explicit wall, with a square array. Goicochea [32] studied the adsorption isotherms of polyethylene glycol (PEG), he has a solute conformed by seven-bead model, a chain where each bead represents a segment of PEG, a solvent with a specific parameter and an implicit soft wall, he studied Lennard-Jones potential also, but only his DPD-like potential for the wall is relevant for this project. To probe that both, our algorithm and our model is correct, we have carried out simulations to compare with the implicit case.

Goicochea's DPD parameters are $\gamma = 4.5$ and $\sigma = 3$ with a timestep $\Delta t = 0.03$, a simulation box with volume $L_x = 5$, $L_y = 5$ and $L_z = 10$. The method used is Hybrid Monte Carlo in the Gran Canonical Ensemble. While the parameter of the conservative force a_{ij} are the following. The particle interaction is 78.0 when $i = j$ and 79.3 for $i \neq j$. While the wall-solvent interaction is 120 and wall-solute interaction is 60.

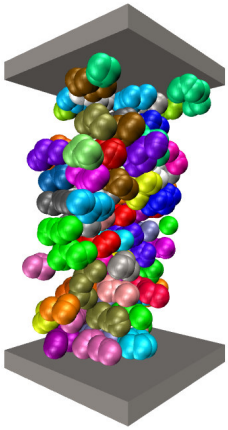

Figure 4.4: Snapshot of the system builded by Goicochea heptamer-like model with implicit walls and a continuos force.

Goicochea uses a DPD-like potential for make a implicit wall, as the following equation

$$F(z) = a_{wj}\left(1 - \frac{z}{z_c}\right), \tag{4.6}$$

where a_{wj} is like the parameter of the conservative force from DPD model for the interaction between the wall and the rest of particles. z is the coordinate for the axis perpendicular to the wall and z_c is the cutting distance.

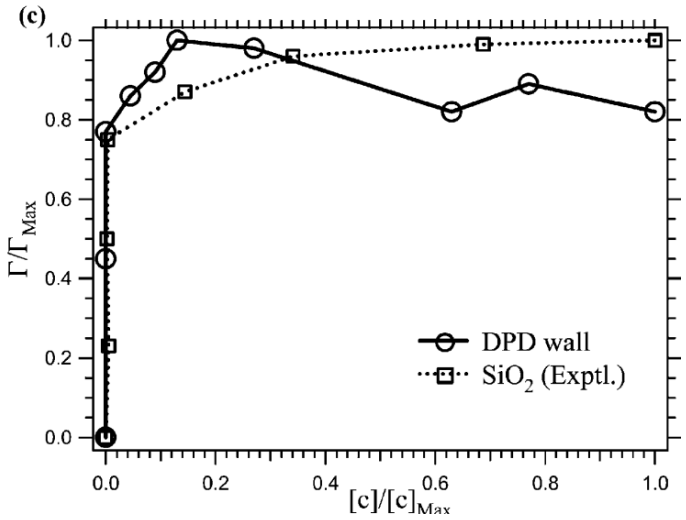

Figure 4.5: Goicochea's plot of the adsorption isotherms extracted from [32] comparing the experimental results with the simulation results with the DPD-like potential. Γ is the adsoprtion isotherm calculated with the expresion in section 3.3.3, [c] represents the value of the density profile in the bulk and $[c]_{Max}$ and Γ_{Max} are their maximum value.

An important difference between Goicochea's system and our system is the wall model. He has a force orthogonal to the wall, the force is continuos over the *xy* plane and along the z axis whereas, we have a discrete force and it extends radially.

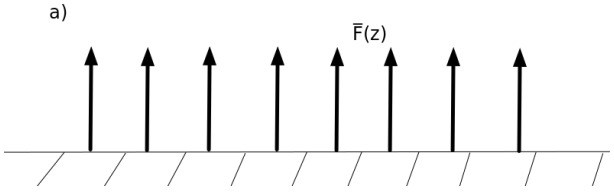

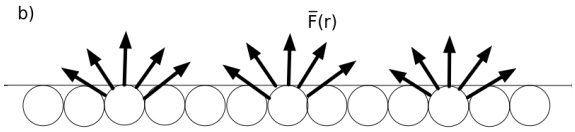

Figure 4.6: a) Scheme of the force field used by Goicochea for the wall model, it is continous in the plane and extends along the z axis. b) Scheme used in our system, it is discrete in the plane and extends radially for each wall particle.

With the previous information we carried out the same system than Goicochea to reproduce the figure 4.5 but, with explicit walls. Our first aproximation was the following. We used a system with a heptamer-like model and a simulation box with a volume of 10x10x10 and explicit walls. The DPD parameters to be equal to Goicochea's, like in table 4.1. The parameters γ and σ are 4.5 and 3 respectively.

a_{ij} interaction	wall	solvent	PEG bead
wall	78	120	60
solvent		78	79
PEG bead			78

Table 4.1: DPD parameter of the conservative force a_{ij}.

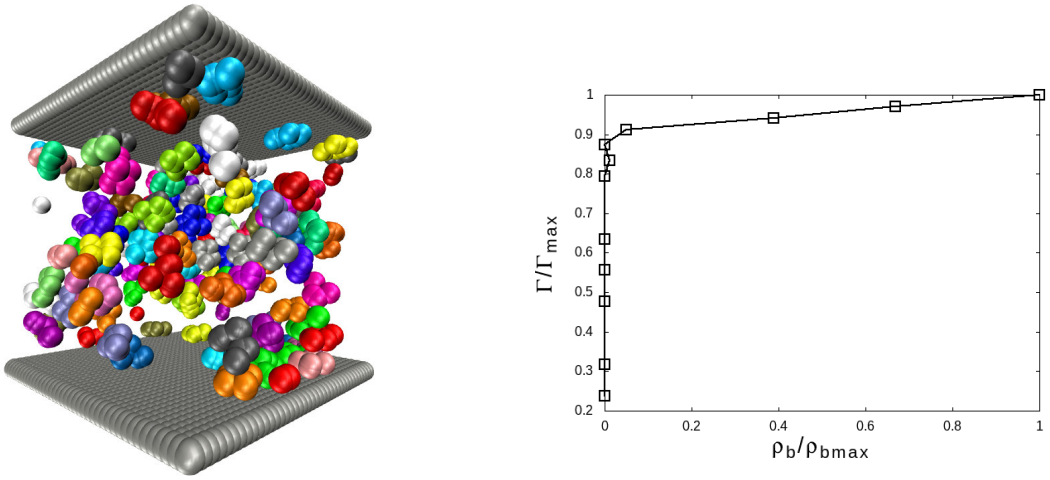

Figure 4.7: Left: Snapshot of the system using heptamer-like model with PEG parameters in a simulation box of 10^3 and explicit walls with $\rho = 3$. color-coded beads represents each 7-chain and the grey beads are the wall particles. Right: Adsoprtion isotherm using the heptamer-like model with PEG parameters in a box of 10^3. ρ_b and ρ_{bmax} are the value of the density profile in the bulk and its maximum.

We obtained the adsoprtion isotherm that we can see in the figure 4.7. We have observed a fast adsorption just like expected by Goicochea's simulations. As chains are progressively introduced, they adsorb onto the surface until a point is reached where the wall undergoes a sudden saturation. It is important to highlight that we are interested in dimers. Therefore, once we replicated the previous results, we opt for study the adsorption of dimer-like model, a simulation box with a volume of 10x10x10 and explicit walls, the DPD parameters equal to Goicochea's.

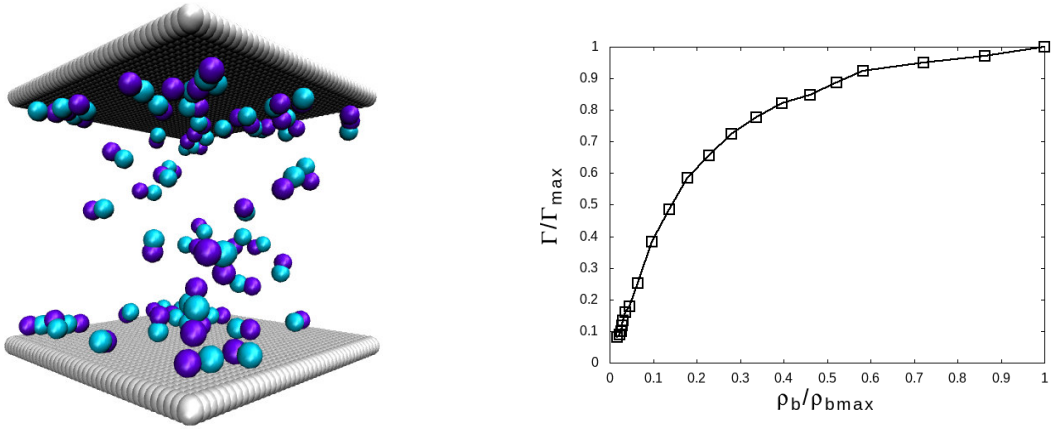

Figure 4.8: Left: Snapshot of the system using dimer-like model with PEG parameters in a simulation box of 10^3 and explicit walls with a $\rho = 3$. Blue beads represents each 2-chain and the grey beads are the wall particles. Right: Adsoprtion isotherm using the dimer-like model with PEG parameters in a box of 10^3 where here ρ_b represents the value of the density profile in the bulk.

In the figure 4.8 we can see that in contrast to the previous case, at low concentrations the dimers adsorb gradually as additional dimers are introduced, resulting in a smoother transition to saturation. The previous results motivated a systematic study of the molecular chain length. The corresponding adsorption isotherm is shown in figure 4.9. It can be observed that the chain length affects the rate at which saturation is reached in the adsorption isotherm. The different cases in figure 4.9 were compared using the same range of ethyleneglycol monomer density in order to ensure a fair comparison.

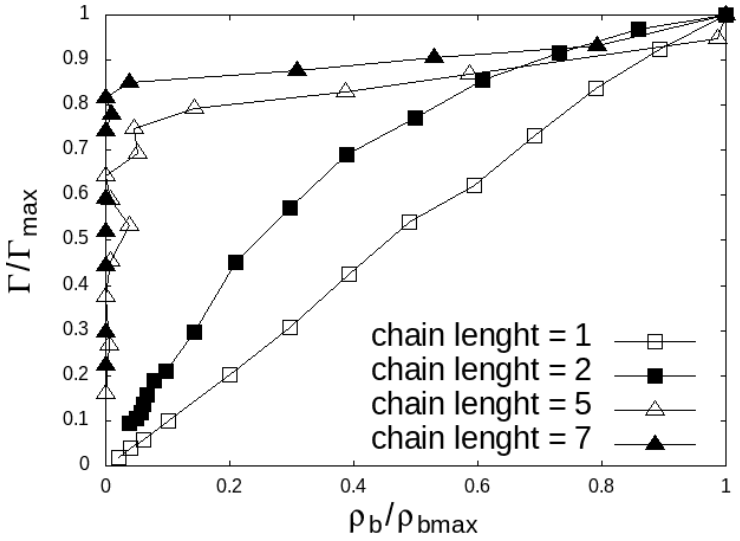

Figure 4.9: Adsorption isotherm normalized with ρ_{bmax} and Γ_{max} with different chain length.

Results are consistently with previous results of Goicochea, more over we have shown the effect of the chain length. Another behaviour that we can see in the previous figures is the transition from an increase adsorption with a zero bulk value for long chains to a flat behaviour in the adsorption as increase the bulk. If we have a short chain you can see a smoth curve, however if we have a long chain you can see a fast transition to flat. In the case of monomers, adsorption exhibits a linear increase, as it is energetically more favorable for them to remain in the bulk. This suggests that short chains tend to stay in the bulk, and a longer chain length is required to promote adhesion. We made simulations with boxes of 5x5x10 like Goicochea, however we have problems, it takes many time to arrive to the equilibrium system, and computing cost. Alternatively it would be necessary to perform a large number of simulations in order to obtain statistically reliable averages. This is because the computing time is longer if we use explicit walls and thats the reason what Goicochea uses implicit wall.

4.3 Fluid Flow Modeling

As we saw in previous sections, bacteriophages infect bacterias. Our approach to model a motile bacteria consist in add a flow to the fluid. This can be done easily with DPD because with this model we can reproduce hydrodynamics interactions, then we can study the adsorption of the virus model with and without flow. To do this, first we want to study the basic and known cases of a fluid between walls using the Navier-Stokes equations. However, although this cases have analytical solutions, we have carried out simulations just with water to reproduce this solutions using the DPD model as a benchmarking.

4.3.1 Navier-Stokes equations

As in many areas of physics, conservation laws are employed, in this case, the conservation of mass. A decrease in fluid mass at a given point in space implies that the mass has been transported to a neighboring region. Letting ρ represent the mass density and $\mathbf{J} = \rho\mathbf{v}$ the mass current density, we arrive to the following expresion.

$$\frac{\partial \rho}{\partial t} + \nabla \cdot (\rho \mathbf{v}) = 0. \tag{4.7}$$

This is the continuity equation wich represents the local conservation of mass [33]. In the case of incompressible fluids $\rho = cte$, therefore the equation reduces to the incompressibility condition

$$\nabla \cdot \mathbf{v} = 0, \tag{4.8}$$

therefore we get

$$\frac{\partial \rho}{\partial t} + \mathbf{v} \cdot \nabla \rho = 0. \tag{4.9}$$

Now, it is possible to use Newton's second law $\mathbf{F} = \frac{d\mathbf{p}}{dt}$ to derive the equation for the momentum of the fluid

$$\int_V \left[\frac{\partial \mathbf{v}}{\partial t} + (\mathbf{v} \cdot \nabla)\mathbf{v} \right] dV = F, \tag{4.10}$$

where F represents the external forces acting on the fluid, among which pressure is one of the most significant contributions. Introducing a pressure P, wich is the force per unit area, therefore we get the Euler equation. While the remaining external forces are expressed in terms of $\mathbf{f}$ as follows

$$\int_V \left[\frac{\partial \mathbf{v}}{\partial t} + (\mathbf{v} \cdot \nabla)\mathbf{v} \right] dV = -\int_S P dS + \int_V \mathbf{f} dV. \tag{4.11}$$

Empirically, it is known that the viscous force is proportional to the velocity of the particles. However, this force must be invariant under Galilean transformations. Since viscosity arises from collisions between particles with different velocities, the viscous force should depend on the rate of change of velocity. Therefore, one might initially assume that it is proportional to the first derivative of the velocity, with vorticity being a natural candidate. Nevertheless, vorticity does not have the same parity as the Euler equation. Consequently, the viscous force must instead depend on second derivatives of the velocity field. In this way, the viscous force can be expressed as $\mu\nabla^2\mathbf{v}$, where μ is the dynamic viscosity constant. Thus, the Navier-Stokes equation [33] is obtained

$$\rho\left(\frac{\partial \mathbf{v}}{\partial t} + (\mathbf{v} \cdot \nabla)\, \mathbf{v} \right) = -\nabla P + \mu\nabla^2\mathbf{v} + \mathbf{f}. \tag{4.12}$$

4.3.2 Couette Flow

One of the simplest cases with an analytical solution to the Navier-Stokes equations is Couette flow. In this case, the fluid is confined between two parallel walls with a separation distance h, where one of the

walls moves at a constant velocity v_w. The analytical solution is given as follows.

Since the fluid is incompressible and there is no pressure gradient, all terms vanish, and the Navier-Stokes equation simplifies to

$$\rho \frac{\partial \mathbf{v}}{\partial t} = \mu \nabla^2 \mathbf{v}. \tag{4.13}$$

It can be inferred that the velocity field has the form $\mathbf{v} = v(y)\hat{\mathbf{x}}$, therefore we obtain

$$\rho \frac{\partial v(y,t)}{\partial t} = \mu \frac{\partial^2 v(y,t)}{\partial y^2}. \tag{4.14}$$

We define the solution as the sum of the steady and transient parts, $v(y,t) = v_s(y) + v_t(y,t)$. Using the boundary conditions $v(0,t) = 0$, $v(h,t) = v_w$, and the initial condition $v(y,0) = 0$, we obtain the steady-state solution ($\partial v/\partial t = 0$):

$$v_s(y) = \frac{v_w}{h} y. \tag{4.15}$$

For the transient part, we introduce it into the partial differential equation as follows

$$\rho \frac{\partial v_t(y,t)}{\partial t} = \mu \frac{\partial^2 v_t(y,t)}{\partial y^2}. \tag{4.16}$$

Defining $\nu = \mu/\rho$, we get the diffusion equation with initial condition $v_t(y,0) = v(y,0) - v_s(y)$.
Using separation of variables $v_t(y,t) = Y(y)T(t)$, we obtain

$$\frac{1}{\nu T}\frac{dT(t)}{dt} = \frac{1}{Y}\frac{d^2Y(y)}{dy^2} = -k, \tag{4.17}$$

where k is a separation constant. Solving each part gives

$$T(t) = e^{-\nu k t}, \tag{4.18}$$

$$Y_n(y) = \sin\left(k_n^{1/2} y\right). \tag{4.19}$$

Non-trivial solutions occur for the discrete values

$$k_n = \left(\frac{n\pi}{h}\right)^2. \tag{4.20}$$

By linear superposition, the transient solution is

$$v_t(y,t) = \sum_{n=1}^{\infty} A_n e^{-\nu k_n t} \sin\left(k_n^{1/2} y\right). \tag{4.21}$$

Using the initial condition and the orthogonality of the sine functions, we find

$$A_n = \frac{2}{h}\int_0^h v_t(y,0)\sin\left(\frac{n\pi}{h}y\right)dy. \tag{4.22}$$

Substituting $v_t(y,0) = -v_s(y)$ yields

$$A_n = \frac{2v_w(-1)^n}{\pi n}. \tag{4.23}$$

Therefore, the complete solution is

$$v(y,t) = \frac{v_w}{h}y + \sum_{n=1}^{\infty} \frac{2v_w(-1)^n}{\pi n} exp\left[-\nu\left(\frac{n\pi}{h}\right)^2 t\right]\sin\left(\frac{n\pi}{h}y\right). \tag{4.24}$$

For long times $t \to \infty$, the exponential terms vanish, and the solution approaches the steady-case profile, this solution is compared with the simulation results. We carried out simulations in a box of 10x11x10, with a $\rho = 4$. In DPD simulations, non-slip boundary conditions can be effectively reproduced by introducing rough, granular walls. We used rough walls with 1500 particles for each wall. We test with differents velocities v_w and we get succesfully the couette flow solution as you can see in figure 4.10

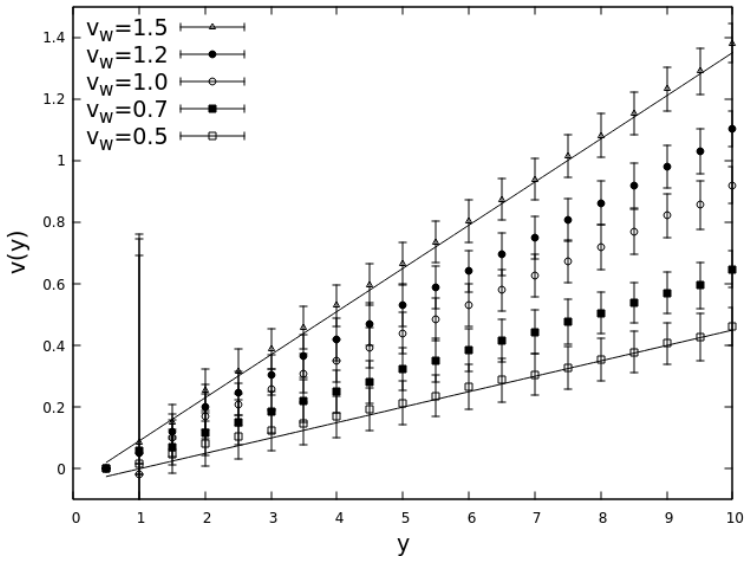

Figure 4.10: Velocities profile for the system with differents velocities v_w. The solid line is a linear fit

4.3.3 Poiseuille Flow

Another analytically solvable case of the Navier-Stokes equations is the Poiseuille flow. This configuration consists of a fluid confined between two parallel walls, one located at $y = h$ and the other at $y = -h$. A constant pressure gradient is applied parallel to the confining walls, so that the induced flow is strictly aligned with the driving force. Under these conditions, the velocity field becomes one-dimensional, $\mathbf{v} = v(y,t)\hat{\mathbf{x}}$, depending solely on the distance from the walls. If the fluid is incompressible, the Navier–Stokes equation reduces to

$$\rho \frac{\partial \mathbf{v}}{\partial t} = -\nabla P + \mu \nabla^2 \mathbf{v}. \tag{4.25}$$

Assuming a unidirectional flow $\mathbf{v} = v(y)\,\hat{\mathbf{x}}$ and a constant pressure gradient along the x direction, $D_x P = cte$, we obtain

$$\rho \frac{\partial v(y,t)}{\partial t} + \frac{dP}{dx} = \mu \frac{d^2 v(y,t)}{dy^2}. \tag{4.26}$$

Applying the no-slip boundary conditions [33], $v(y = \pm h, t) = 0$, and considering the stationary limit ($\partial v/\partial t = 0$), we find the steady-state solution

$$v_s(y) = \frac{1}{2\mu}\frac{dP}{dx}\left(y^2 - h^2\right), \tag{4.27}$$

where the maximum velocity occurs at the channel center ($y = 0$) and is given by

$$v_{s,\max} = -\frac{h^2}{2\mu}\frac{dP}{dx}. \tag{4.28}$$

The maximum steady-state velocity $v_{s,\max}$ is determined by the magnitude of the applied pressure gradient $D_x P$. This gradient constitutes the primary input parameter governing the Poiseuille flow conditions in our setup and is the value explicitly prescribed in the simulations discussed later. We define the total velocity as the sum of the steady and transient components,

$$v(y, t) = v_s(y) + v_t(y, t). \tag{4.29}$$

Substituting into the governing equation, we obtain

$$\frac{\partial v_t(y, t)}{\partial t} = \nu\frac{\partial^2 v_t(y, t)}{\partial y^2}, \tag{4.30}$$

which corresponds to the diffusion equation with $\nu = \mu/\rho$.

Using separation of variables, $v_t(y, t) = Y(y)T(t)$, together with the boundary conditions $v_t(\pm h, t) = 0$ and the initial condition $v_t(y, 0) = v(y, 0) - v_s(y)$, we find the transient solution

$$v_t(y, t) = \sum_{n=1}^{\infty} B_n\, e^{-\nu\lambda_n t} \sin\left[\lambda_n^{1/2}(y + h)\right], \tag{4.31}$$

where the eigenvalues are

$$\lambda_n^{1/2} = \frac{n\pi}{2h}, \tag{4.32}$$

and the coefficients are determined from the orthogonality of the sine functions as

$$B_n = \frac{1}{h}\int_{-h}^{h} v_t(y,0)\sin\left[\frac{n\pi}{2h}(y+h)\right]dy. \tag{4.33}$$

For long times ($t \to \infty$), the transient terms vanish, and the velocity field approaches the steady parabolic Poiseuille profile. As in the Couette flow case, the steady solution is compared with the simulation results. The same system with $\rho = 4$ in a simulation box of size 10x11x10 was used. The numerical solutions obtained are shown in Figure 4.11 showing the parabolic solution.

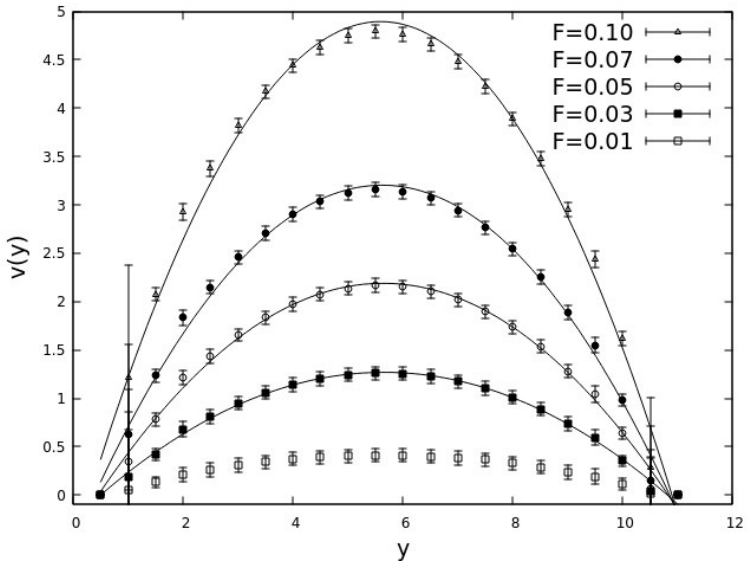

Figure 4.11: Velocities profile for the system with differents constant forces introduced $F = -\nabla P$. The solid line is a quadratic fit.

It should be noted that, in the analytical framework, a pressure gradient appears explicitly in the Navier–Stokes equations. In contrast, in simulations, this pressure gradient is implemented as a constant external force applied to each fluid particle.

It is important to emphasize that, in order to reproduce these flows,

it was necessary to model the boundary conditions within DPD. To achieve this, rough walls were implemented in the simulation box, providing an alternative to other available approaches [34].

Chapter 5

Static Case

5.1 Abstract

This section presents the results obtained using the tools described in Section 3.3, with the aim of elucidating the infection dynamics of the phage. However, it is important to note that this work can be considered a basic science study. Since the system consists of dimers embedded in a surrounding fluid and confined between two walls. While the model is general in nature, it holds the potential to contribute to the understanding of phage infection dynamics.

The results will be presented in this section. They include the analysis of the dynamics through the mean square displacement of the dimers' center of mass, as well as the density profiles for different cases, such as amphiphilic and neutral walls. These results provide insight into both the dynamical and configurational behavior of the system. Orientational order parameters like the polar order, wall order and nematic order to caracterize the infection by bacteriophages. Another topic of interest is the adsorption on the wall, this is caracterized with the density profile and adsorption isotherms. Finally the adsorption time wich it is relevant since the system is very dynamic, therefore we define a way to compute

the adsorption time for the dimer.

5.2 Simulations Details

All parameters are given in DPD units. The system consist in a cubic simulation box with length of $20r_c$, in DPD units, for the study of figures 5.1 and 5.2, and length of $10r_c$ for the rest of simulations. As we comment in section 3.1 and 3.2, we have particles that represents the fluid, with dimers that represents the bacteriophage embbeded in the fluid. In the xz plane, two walls are placed at the extremes along the y-direction, composed of DPD beads. Only DPD interactions are considered between all beads. Due to the way the virus is modeled, each DPD bead represents approximately 100 nanometers.

5.3 Hydrophobic Interaction of the Walls

We are building the system from the foundation. The cell membrane surface is hydrophilic in the nature. To understand the interaction with walls we have carried out a systematic study with differents repulsion parameters and modifying the hydrophobicity. In the nature the cell membrane is made by many different components like phospholipid molecules, proteins, salts, etc. All this components modify the pH around the fluid, playing an important role in the infection by phages. If we add salts, we need to add electrostatic interactions, with a high computing cost, therefore we make a systematic study for the net hydrophobicity in mesoscales to consider all the aforementioned factors. This is a heuristic study, without an exact or detailed mapping to a specific biological system. For the moment, our focus is on a basic science model consisting of walls and embedded dimers. However, the study of virus–bacteria interactions will be revisited later in this work.

First, to characterize the effect of the harmonic constant k on the dynamics, we made some simulations with differents harmonic constants. The simulations were made with a cubic simulation box with a length of 20. Each wall was made with a square arrangement and 6400 particles. 6000 dimers and 12000 solvent particles. The DPD parameters are in the table 5.1. The value for γ is 4.5 for all the cases. The a_{ij} for the wall-wall interaction is not relevant because the walls are static.

a_{ij} interaction	Wall	Solvent	Head	Tail
Wall	25	50	50	25
Solvent		25	25	25
Head			25	50
Tail				50

Table 5.1: DPD parameters for the a_{ij} interaction for each type of bead in the simulation. For all interactions $\gamma = 4.5$, $\sigma = 3$ and $K_BT = 1$.

The results for the mean square displacement, as defined in Section 3.3.1 (Figure 5.1), were computed in two dimensions, in the xz plane. The MSD's show no significant variation for different values of the harmonic constant k defined in (3.1). Therefore, this parameter can be disregarded, as it does not have a relevant impact on the system's dynamics.

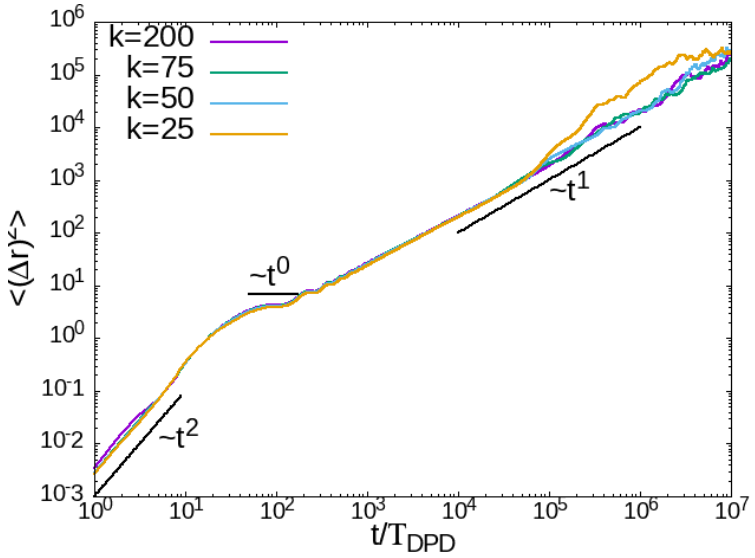

Figure 5.1: Mean square displacement of the center of mass of the dimers in logarithmic scale with different harmonic constant and $l_0 = 0.5$, l_0 is defined in (3.1). The power n of t for each line segment is written on the plot. T_{DPD} is the characteristic time scale of the DPD phenomenon.

However, as in figure 5.1 and 5.2 we have three different types of diffusion, where $n = 2$ it is due to the balistic behavior of the start of the simulation. Where $n = 0$ is a transition to the state of $n = 1$ that is when the system is termalized. In figure 5.2, the case of $k = 200$ you can see a little gap at $t = 10$ corresponding to the displacement for each dimer to the position of equilibrium due to the high harmonic constant and a $l_0 = 1$.

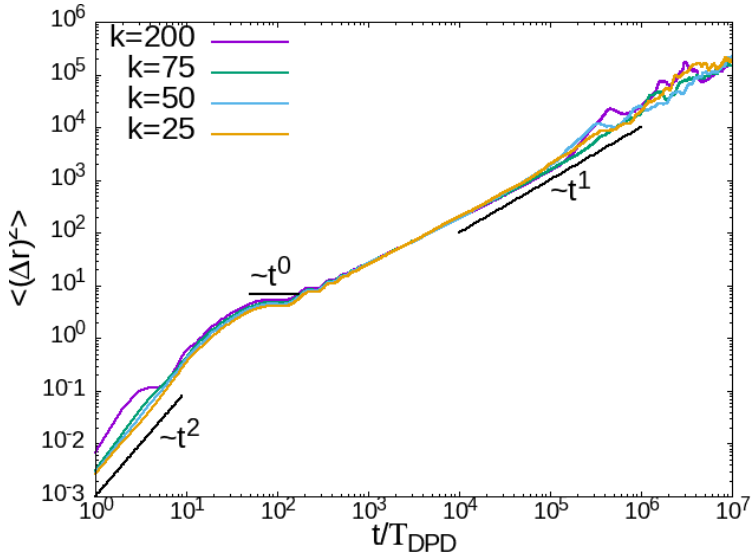

Figure 5.2: Mean square displacement of the center of mass of the dimers in logarithmic scale with different harmonic constant and $l_0 = 1.0$. The power of t for each line segment is written on the plot.

Now, we define our system with a intermediate $l_0 = 0.7$ and a harmonic constant $k = 200$. Then we reduce the system to a cubic simulation box with length of 10^3. Therefore we modify the wall to 1600 beads for each wall, that is to say 3200 wall particles, 3000 solvent particles and 80 dimers, that is to say 80 heads and 80 tails.

We carry out four types of simulations: Hydrophilic-H consists in a hidrophilic wall but with high repulsion to the head. Hydrophobic-T consist in a hydrophobic wall with high repulsion to the tail. W25 consist in a simulation where the wall has the same interaction with all the beads, with value of 25 for the repulsion. W75 is the same idea than W25 but with value of 75 for the repulsion. Therefore we modify systematically the parameter as the table 5.2.

a_{ij} interaction	wall	solvent	head	tail
wall	25	25/75/25/75	75/25/25/75	25/75/25/75
solvent		25	75	25
head			75	75
tail				75

Table 5.2: DPD parameters of the conservative force a_{ij} with different models. In each case, a specific color was assigned to represent the interactions: red for hydrophilic-H, blue for hydrophobic-T, green for W25, and violet for W75.

The MSD obtained for these systems were very similar for each model as you can see at figure 5.3. The system exhibits highly dynamic behavior, involving three distinct types of force field parameters.

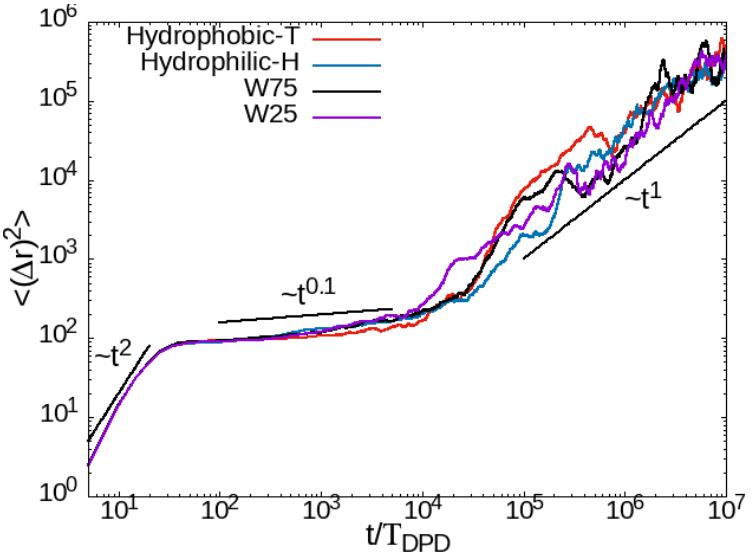

Figure 5.3: Mean square displacement of the center of mass of the dimer in logarithmic scalefor each case. The power n of t for each line segment is written on the plot.

You can see three regimes in the MSD, where $n = 2$ is due to the first timesteps of the simulations when the virus start to move, since the MSD is being calculated only in the xz plane, when $n \approx 0$ is due to a trasient state, the dimer are moving along of y to be closer to the walls,

therefore we are not measuring this dynamics. The length of this state is due to the time it takes for the dimers to settle on the wall. Then $n = 1$ because once we have the dimers in the state of minimum energy, they start to move with a diffusion proportional to t.

Thanks to the MSD results we can say that the diffusion is the same in the xz plane in the different cases, therefore the difference between each case should be in the adsorption to the walls, since walls are different. Once we measure the diffusion by the dimers, we can measure the orientation by the dimers, where the orient depends on the repulsion parameters.

We did not measure the MSD near the wall. Although we understand that such measurements would provide more detailed insights into the system being characterized, the high dynamical nature of the system makes it very challenging to obtain data in that region. However, in the following sections, we present an alternative observable calculated as a consequence of this limitation.

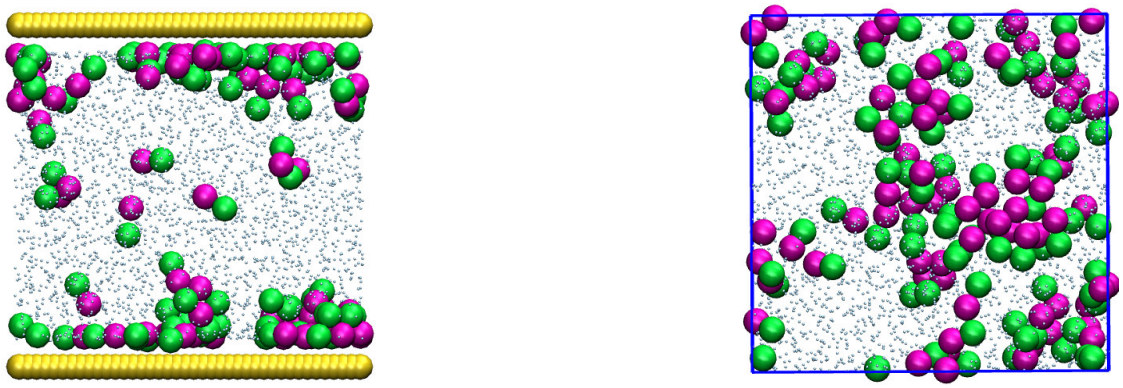

(a) (b)

Figure 5.4: Snapshots of the simulation box of the Hydrophilic-H case. The fluid is represented by smaller blue beads for visualization reasons. The yellow beads represent the wall. The purple beads correspond to the heads of the dimers. The green beads represent the tails of the dimers. a) *xy* plane. b) *xz* plane.

(a) (b)

Figure 5.5: Snapshots of the simulation box of the Hydrophobic-T case. The fluid is represented by smaller beads for visualization reasons. a) *xy* plane. b) *xz* plane.

As you can see in figure 5.4, aggregates form near the wall due to the evident tendency of the particles to move towards it. However, in Figure 5.5, there is also a clear tendency toward the wall, but an implicit orientation can be observed as well. We have carried out the simulations in W25 and W75 cases, but the snapshots are a intermediate cases be-

twteen the previous figures, you will see the cases in the density profiles.

In Figure 5.6, the orientation can be observed in both cases, with a more pronounced alignment in the Hydrophobic-T case. However, we also observe a situation in which the head is positioned closer to the wall than the tail. This is not the desired configuration, as phage infection occurs through the tail.

The W25 and W75 cases, shown in Figure 5.7, represent a mixture of the previous scenarios. The orientation is nearly imperceptible, similar to the Hydrophilic-H case. However, unlike the Hydrophobic-T cases, there is no formation of a second layer of heads near the wall. However, you can see that in figure 5.6b, the peak is higher than 5.6a due to value of the bulk in both cases. While in figure 5.7 the difference in the height is due to the width of the peak, in figure 5.7a is wider, therefore decreases the height of the peak to preserve density. It is also noteworthy that, in these cases, the heads approach the wall more closely than the tails, despite the fact that, according to the parameters in table 5.2, the heads are always hydrophobic and the tails are always hydrophilic.

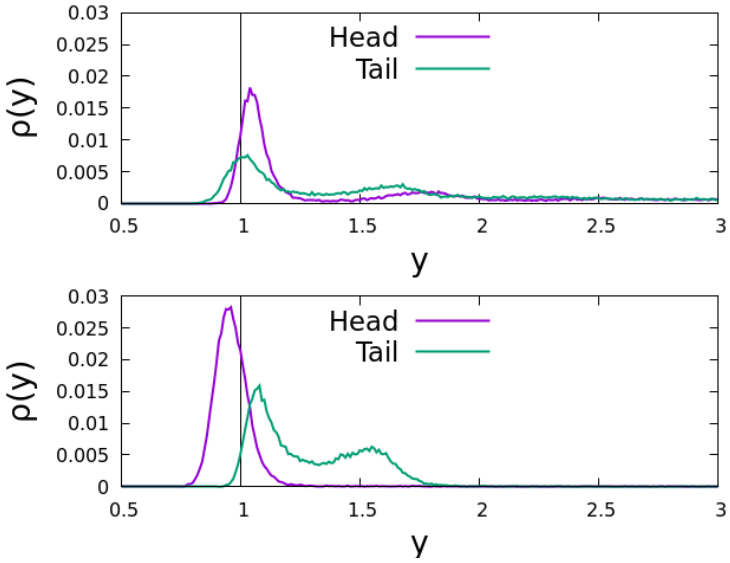

Figure 5.6: Density profile of head and tail of the dimer. a) Hydrophilic-H case. b) Hydrophobic-T case. A solid line at $x = 1$ is included to facilitate the visualization of the orientation.

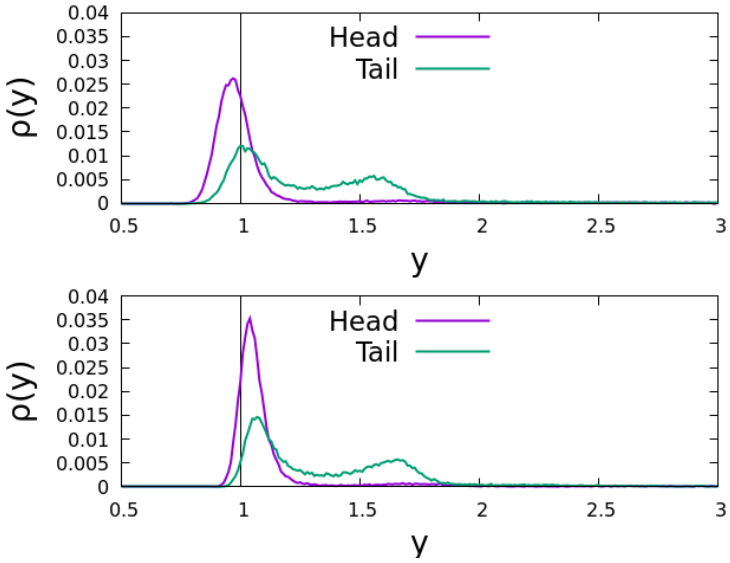

Figure 5.7: Density profile of head and tail of the dimer. a) W25 case. b) W75 case.

In figure 5.8 you can see all the cases together, where you can see the small second layer in Hydrophilic-H case for the heads, but for the

tails there is always a hydrophilicity, where the layer closer to the wall is higher.

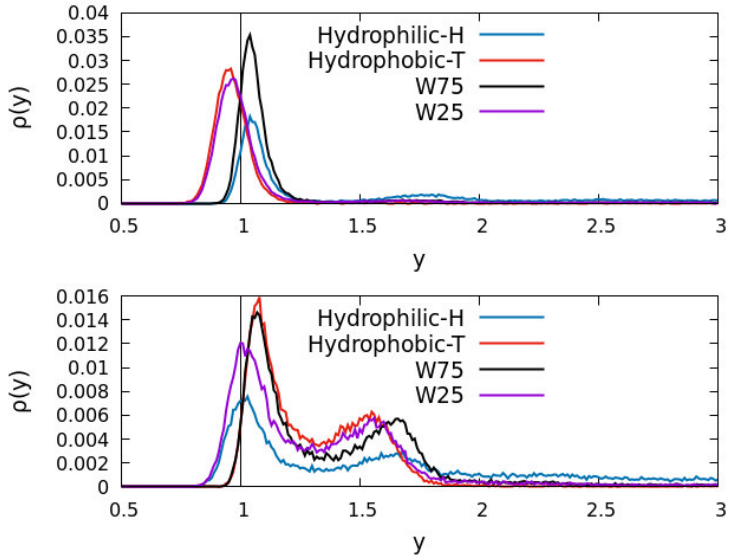

Figure 5.8: Density profile of all the cases. a) head profiles. b) tail profiles.

We have covered all posible scenarios. The phage infects with the tail, therefore there is a factor that we are not seeing. Therefore we opt for study a simpler system. Let's go one step further, we will remove the hydrophobicity and study a system with a different repulsion to the tail, giving us a implicit atraction to the tail. This system is studied in the following subsection.

5.4 Heterogeneus Walls

Now we will study a system like the previous subsection but we remove the hydrophobicity and use a neutral case where we put another type of bead that represents the affinity zone in the cell wall by the tail. Therefore the wall is conformed by two types of bead, we vary the affinity zone concentration called χ. Where $\chi = 0.00$ represents the absence of

affinity zone and $\chi = 1.00$ is when all the wall is affine to tail beads. In the nature the affinity zones usually have specific proteins. We put a higher repulsion in the head-head, tail-tail and protein-head interaction. Additionally a lower repulsion in tail-protein interaction.

a_{ij} interaction	Wall	Solvent	Head	Tail	Affinity Zone
Wall	75	75	75	75	75
Solvent		75	75	75	75
Head			**150**	75	**150**
Tail				**150**	**25**
Affinity Zone					75

Table 5.3: DPD parameters for the a_{ij} interaction for each type of bead in the simulation. For all interactions $\gamma = 4.5$, $\sigma = 3$ and $K_BT = 1$.

As you can see, the objective of this configuration is to model the adsorption competition between affine and non affine area. To make a simpler system we opt for a circular area in the middle of the simulation box, we vary its radious systematically. In figure 5.9 you have a visualization of the simulation box.

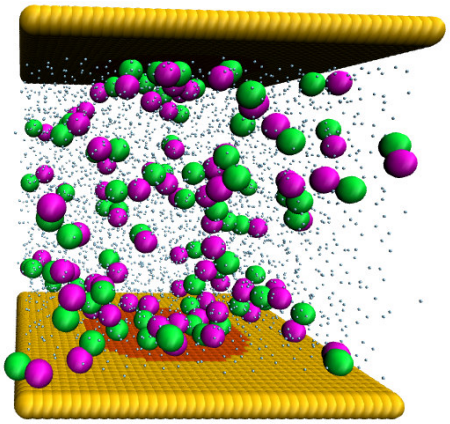

Figure 5.9: Snapshot of simulation box with the dimers embedded in the solvent. The solvent is confined by the cell walls with affinity zone (red beads).

As result we have measured the density profiles and some orienta-

tional parameters discussed in the section 3.3. Obtaining the following plots.

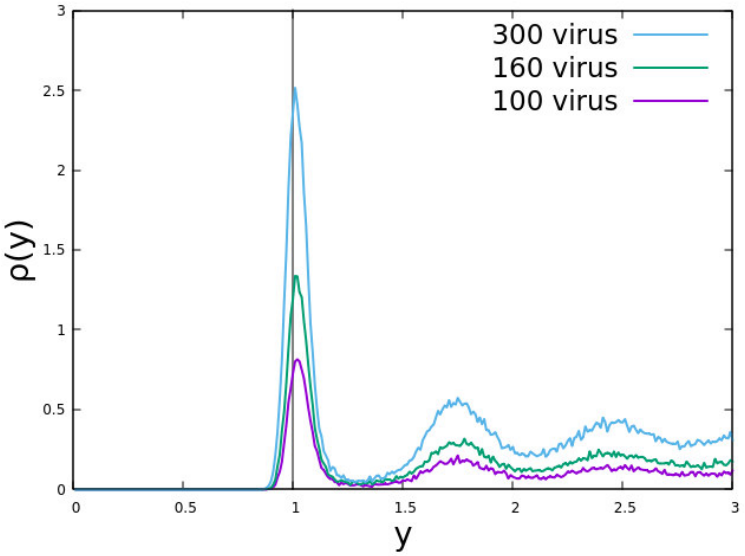

Figure 5.10: Tail density profile of dimers with 3 values of viral load and $\chi = 0.00$.

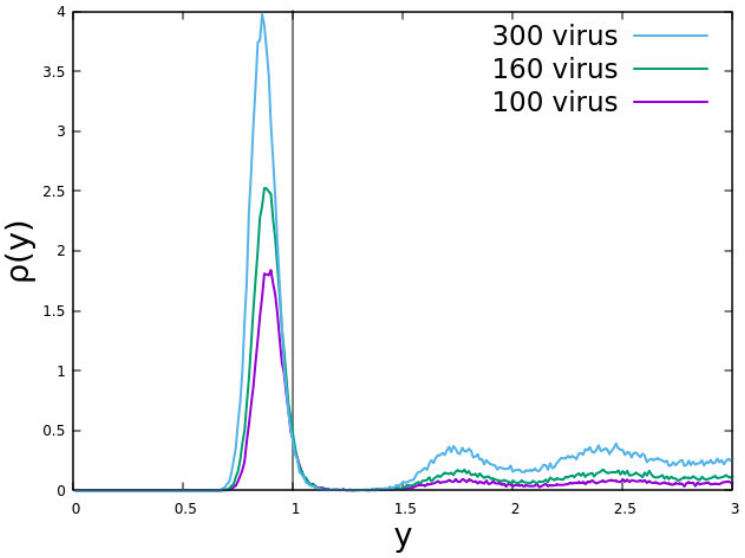

Figure 5.11: Tail density profile of dimers with 3 values of viral load and $\chi = 1.00$.

As you can see in figure 5.10 and 5.11, there is an increase of the

layer adsorbed as increases the viral load and other values of χ are intermediate cases of these. You can also observe that the adsorption peak for $\chi = 1.00$ is higher than for $\chi = 0.00$. As a consequence, the bulk density in the $\chi = 0.00$ case is higher. If we use the equation

$$\Gamma(\rho_b) = \int_0^L [\rho(y) - \rho_b]\, dy, \tag{5.1}$$

we are considering information of all the system, the density profile in the complete box and the increament of the bulk concentration.

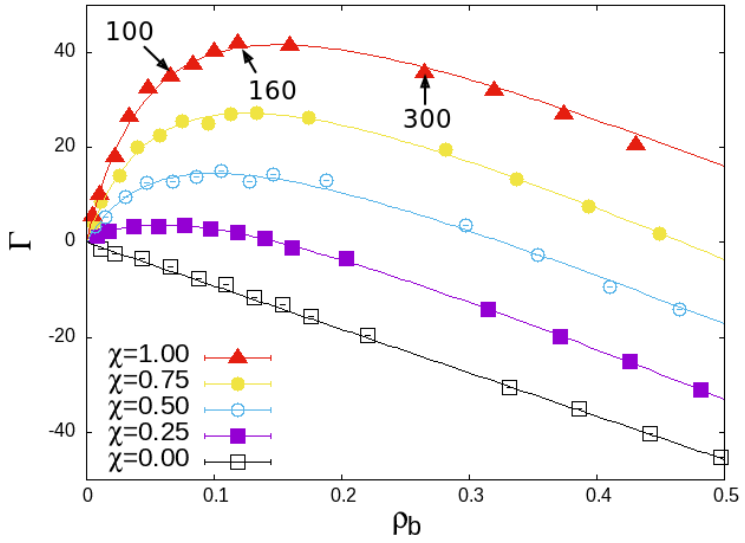

Figure 5.12: Plot of adsorption isotherms Γ with different χ. The three points marked with arrows correspond to 100, 160, and 300 viruses in the simulation box. The solid line is a fit using the equation (5.2)

We do not have a saturation in the isotherm due to the screening effect of the dimers because the dimers are heterogeneus, we obtain a saturation in the case of homogeneous dimers in the benchmarking section, figure 4.9. Given the nature of the adsorption process, the data were fitted using a two-term model: a Langmuir-type term and a linear

term, as shown in the following equation.

$$\Gamma(\rho_b) = \Gamma_{max}\frac{k_L\rho_b}{1 + k_L\rho_b} - \alpha\rho_b \tag{5.2}$$

where Γ_{max} denotes the maximum adsorption, k_L is the Langmuir adsorption constant, and α is the weighting coefficient associated with the linear term.

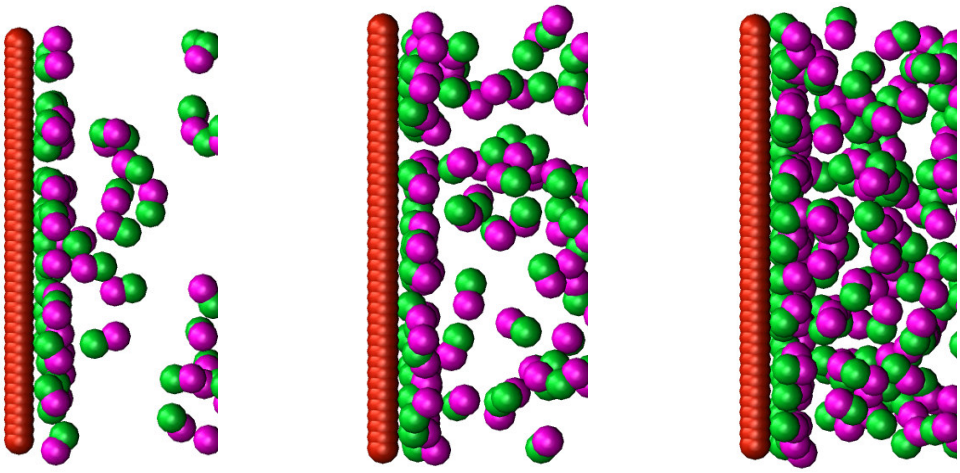

(a) (b) (c)

Figure 5.13: Snapshot of the highlighted cases in figure 5.12 for $\chi = 1.00$. (a) 100 virus. (b) 160 virus. (c) 300 virus.

However we have to be careful in the interpretation because in figure 5.12 you can see that there are points with the same value of Γ, like the marked points with an arrow with 100 virus and 300 virus. You can see that Γ decreases as the viral load increases up to 160 virus. This behaviour is easy to explain in terms of density profile of figure 5.11, there are other layers after the highest peak (300virus). The combined value of the integral over the bulk region and the second peak of the blue line is approximately equal to the integral over the first purple peak alone, resulting in the same net adsorption in both cases. In figure 5.13 the snapshots of the discussed cases are shown, where the increase in both,

the adsorbed dimers and the bulk can be more easily observed visually.

An interesting result is observed in figure 5.10 and 5.11, you can see the difference between the position of the first peak at $y = 1$. The peak was closer to the wall when $\chi = 1.00$ as it is expected, however the second peak is in the same position in both cases of χ. This behavior is due to the lower repulsion from the wall, which allows the tails to come closer to the surface, therefore a layer by heads is formed. This modifies the net interaction with the dimers in the bulk. Conversely, when the wall exhibits stronger repulsion, a sparse layer of heads is formed near the surface. In both cases it turns out that the net interaction between the second layer and the wall is the same due to the screening effect.

Alternatively, we can compute the absolute adsorption isotherm, since experimentally, they count the concentration of adsorbed particles, therefore if we want to compare the results we need to use this second definition using an adsorption gap b:

$$\Gamma_{abs}(\rho_b) = \int_0^b \rho(y)dy \tag{5.3}$$

If we see the density profile, we can define $b = 1.3$ to consider only the first peak, with this definition of Γ_{exp} the results are the following

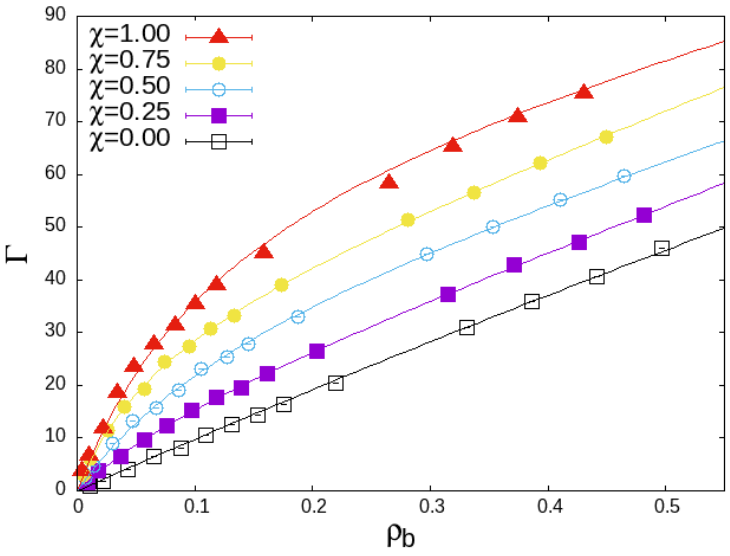

Figure 5.14: Plot of adsorption isotherms Γ_{abs} with different χ, computed as in equation (5.3).

In figure 5.14 you can see that Γ_{abs} grows monotonically, this does not necessarily correspond to reaching a maximum adsorption capacity Γ_{max}.

Now we will introduce another obervable, the orientation. An orientation emerges naturally due to the heterogeneity of the interactions between dimers and walls. To characterize such orientation let explain the density profiles first. This becomes evident when analyzing the density profiles for a wider range of viral load cases and for the two extreme values of χ, as shown in the following figures.

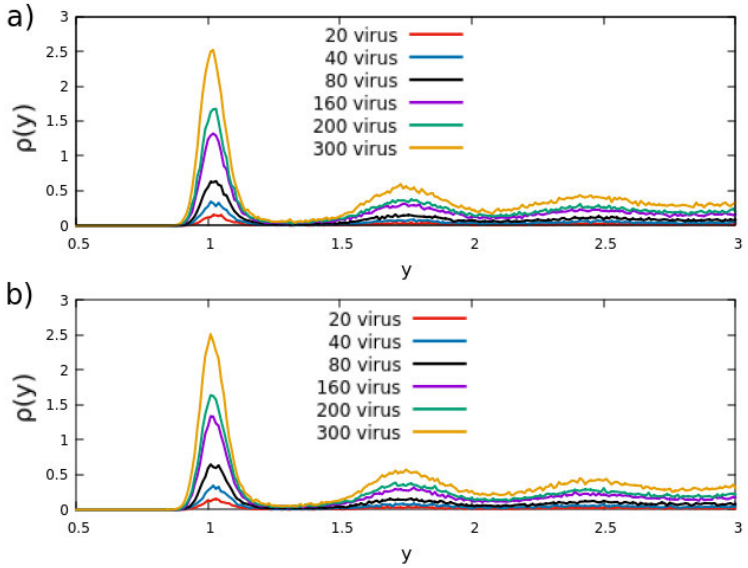

Figure 5.15: Density profile of dimers with different viral load with $\chi = 0.00$. a) Head profiles. b) Tail profiles.

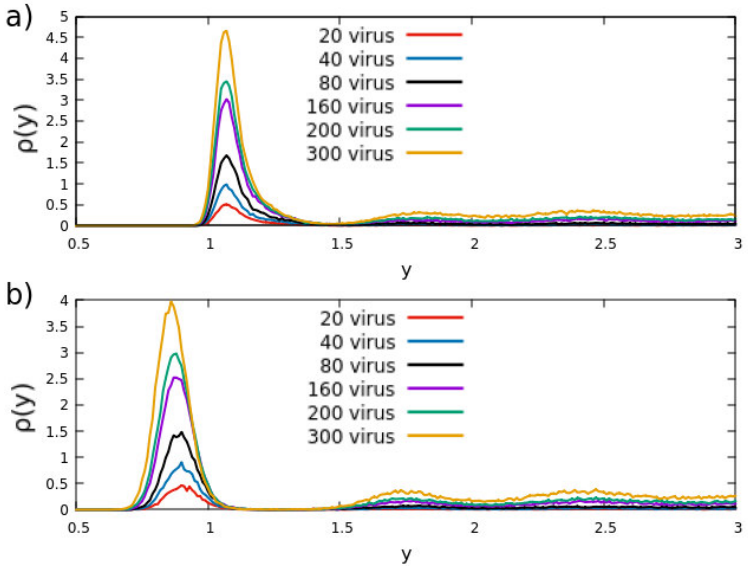

Figure 5.16: Density profile of dimers with different viral load with $\chi = 1.00$. a) Head profiles. b) Tail profiles.

Now, in figure 5.15, no preferential orientation is observed, as the wall lacks affinity regions. Adsorption is present, however, the heads

and tails remain at the same level. In 5.16, you can highlight that there is an emergent orientation by the displacement in the adsorbed layers due to $\chi \neq 0$. The maximum value of figure 5.16a is shifted with respect to the maximum value of figure 5.16b. This indicates that the dimers adopt a preferential orientation, in which the tails tend to be closer to the wall than the heads, thus giving rise to an emergent orientation. This make us to think how can we measure the orientation. Two parameters are chosen to measure both polarity and alignment, the Polar-Order and the Wall-Order discussed in section 3.3.

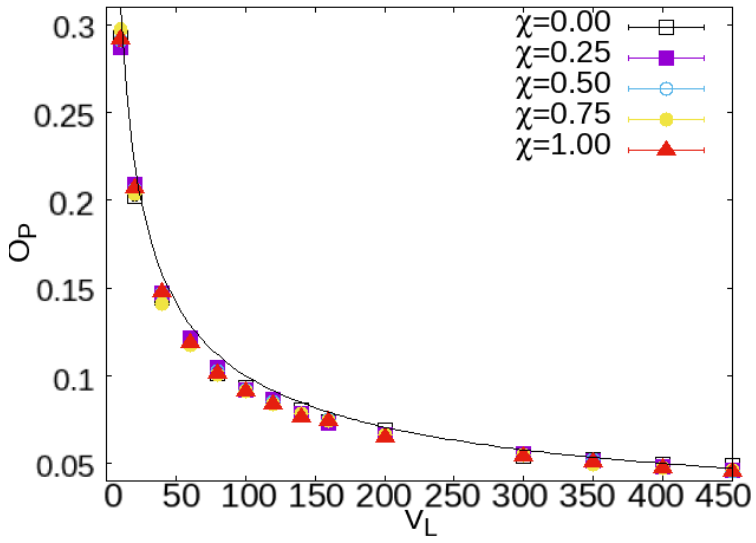

Figure 5.17: Global Polar-Order with different values of χ. Varying the viral load in x-axis. Error bars are smaller than the symbol size. Solid line is the function $1/V_L$ where V_L is the viral load.

In figure 5.17, the global polar order is plotted. This is calculated by assigning to each dimer a vector that points from the tail to the head. The global polar order is computed using all the dimers in the simulation box, that is, both the adsorbed and those in the bulk. It can be observed that the global polar order does not show any variation with respect to χ, since, although there is alignment in the affine regions, it

is compensated by the randomness in the bulk and the non-affine regions, thus maintaining the same global polar order, more over polarity on walls cancels each other. The behavior was fitted using the function $1/\sqrt{V_L}$, consistent with expected scaling laws.

Alternatively, the polar order was computed by considering only the dimers located near the wall, figure 5.18. Under this criterion, the polar order shows a χ-dependent behavior, increasing with higher values of χ. The polar order displays a trend resembling the decay of $1/\sqrt{V_L}$. Nevertheless, for $\chi = 0.5$ the decay levels off, forming a plateau, while for $\chi > 0.5$ an increase in the polar order is observed

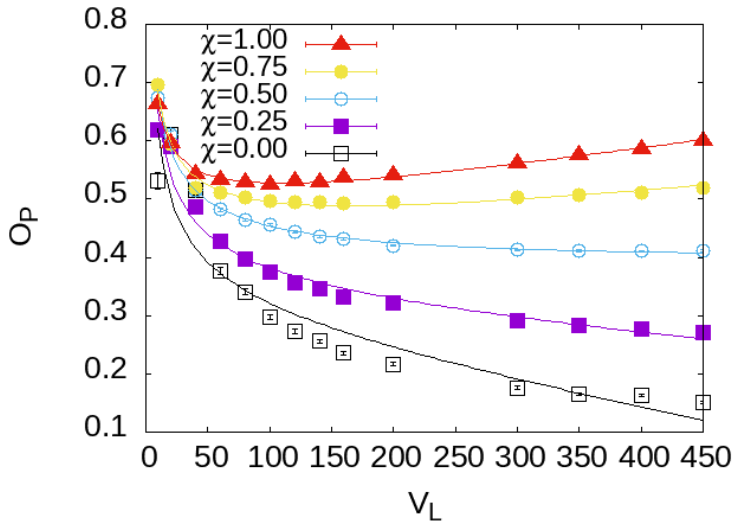

Figure 5.18: Polar-Order close to the wall with different values of χ. Varying the viral load in x-axis. Error bars are smaller than the symbol size. The solid lines are the fits by equation (5.4).

The observed behavior indicates that for small values of V_L, the polar order follows a $1/\sqrt{V_L}$ scaling, suggesting the dominance of random fluctuations. In contrast, for large V_L, a linear increase becomes evident, pointing to a different mechanism driving the alignment. As a result, a reasonable fit can be achieved using a linear combination of these two

functional forms, as illustrated in Figure 5.18. The fit equation is the following

$$O_P(V_L) = \frac{a}{\sqrt{V_L}} + bV_L + c, \tag{5.4}$$

where $O_P(V_L)$ is the polar order in function of the viral load, a, b, c are fitting parameters. In figure 5.18, at $\chi = 0.5$, we observe a transition in which the influence of the linear term in the fitting equation becomes more significant.

With respect to the Wall-Order measured close to the wall, figure 5.19, this is an orientation with respect to the wall therefore, we have a consistent result, there is more orientation with more affinity zone. The increament in the wall order for systems with $\chi > 0.5$ can be understood in terms of entropic effects. As the viral load grows, dimers become increasingly crowded near the wall, leading to alignment driven by the steric pressure exerted by neighboring particles. In the case of $\chi = 0.25$ the wall order decreases as the viral load increases, since wall is dominated by no-affine zones, therefore no alignment is observed. whereas at $\chi = 0.50$ a crossover is observed. For $\chi = 0.0$, the system exhibits a flat response.

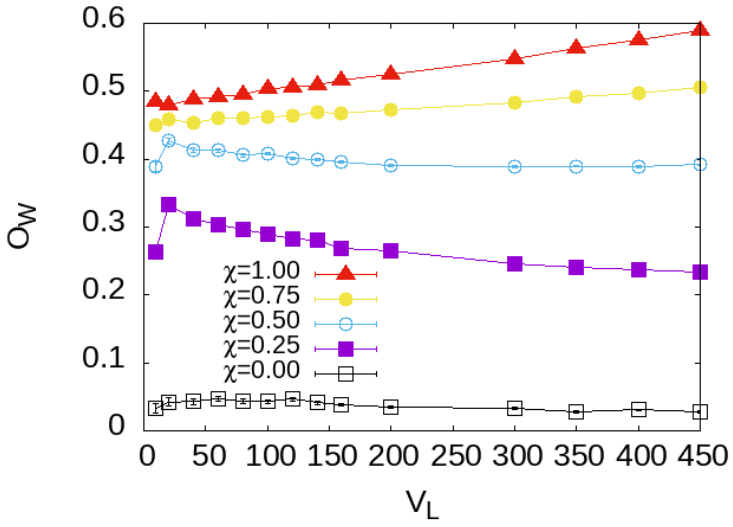

Figure 5.19: Wall-Order with different values of χ. Varying the viral load in x-axis. Error bars are smaller than the symbol size.

Once we computed the adsorption isotherm and the Wall-Order. It is known that, in nature, phages tend to ”walk” along the cell membrane prior to infection [35], moving over the polysaccharides present on the bacterial surface. How can we simulate this phenomenon? Our model is highly dynamic; thus, phages may be near the wall at one time step and far from it in the next. To quantify this behavior, we propose measuring the number of dimers close to the wall at each time step.

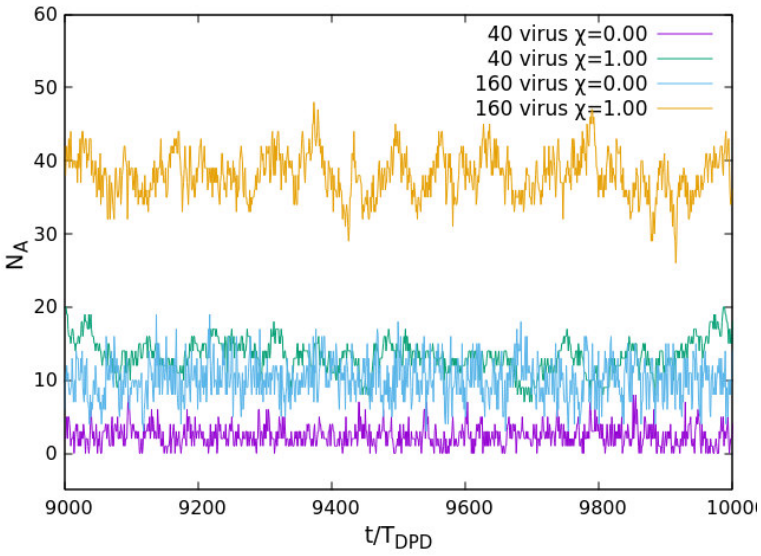

Figure 5.20: Number of adsorbed dimers for each time step with two viral loads and the two extreme values for the affinity zone. τ_{DPD} is the characteristic time of the phenomena.

In figure 5.20 you can see that the number of adsorbed dimers is stable with a little of noise. We can also characterize the time average A_t that dimers keep adsorbed. When the dimers approaches to the wall (with a defined gap) we start counting the A_t, the dimer "walk" on the wall, when the dimer moves away from the wall we stop counting. We calculate the average over all the adsorbed dimers.

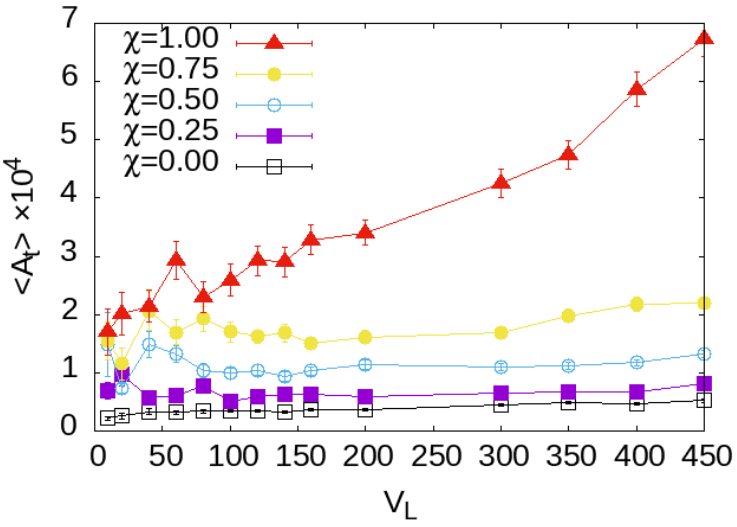

Figure 5.21: Average adsorption time $\langle A_t \rangle$, varying the viral load and different cases for χ.

As you can see in figure 5.21 the adsorption time is constant up to $\chi = 0.75$. Above this value, the adsorption time increases as the viral load increases. This behavior arises from the transition to a homogeneous wall. In the case of a heterogeneous wall, certain regions repel the dimers, limiting their adsorption. The heterogeneity creates a region for dimer exchange, i.e., where $\dot{N}_A = cte$. In contrast, a homogeneous wall promotes sustained adsorption, this is because the entire wall is less repulsive and does not contain regions that would drive the dimers into the bulk. The adsorption time increases as the number of dimers in the system grows.

Another interesting observables are the correlation functions [36], as the equation (5.5), it is a way to know the dynamical behaviour of the system in a specific region, where we can get information about the memory system. In our particular case, we are interested in the velocity autocorrelation function $C_v(\Delta t)$ given the sample data that we have access. Correlation results were computed for $\chi = 1.00$

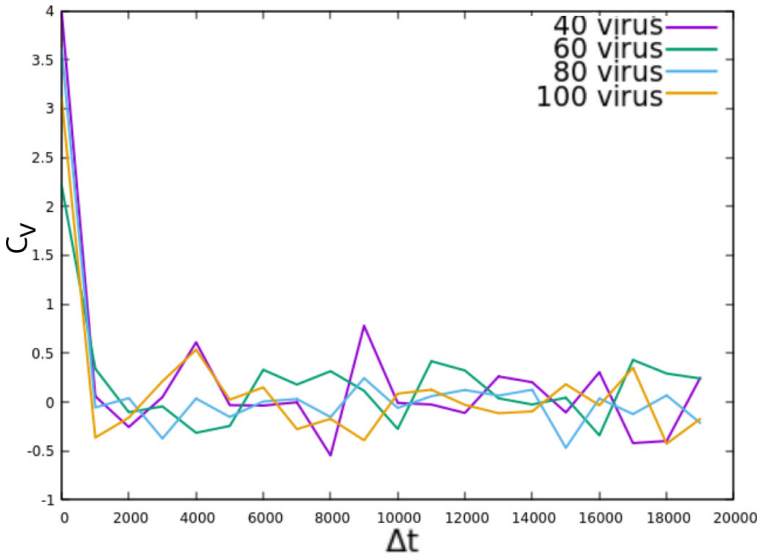

Figure 5.22: Velocity autocorrelation function $C_v(\Delta t)$ with different values for viral load, 40, 60, 80 and 100 virus.

As you can see, there is not correlation for all the cases despicted in figure 5.22. The function instantly decays to zero.

Taking advantage from this, we calculate the directional correlation function $C_d(\Delta t)$, figure 5.23. The result shows us a small correlation, there is an instant decay to $D_d \approx 0.25$ and the behaviour is very similar for different viral loads.

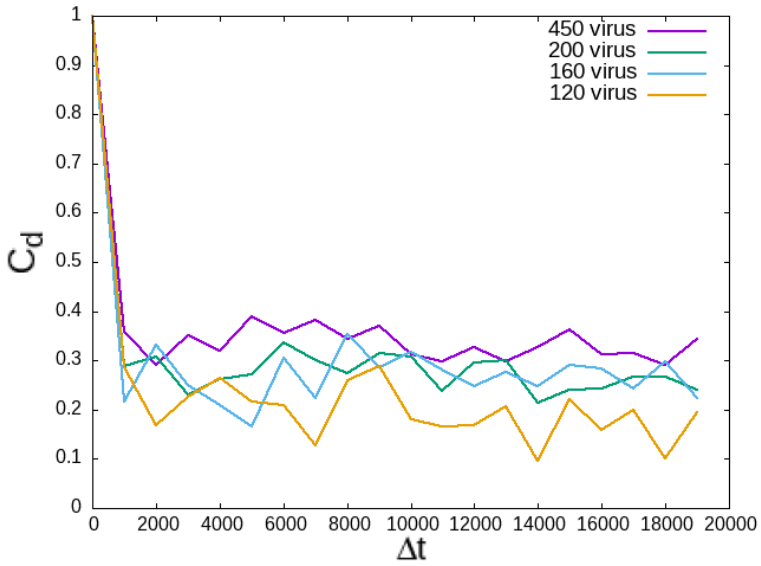

Figure 5.23: Directional correlation function with different values for viral load, 120, 160, 200 and 450 virus.

The expression for both correlation functions is given by the following equation

$$C_x(\Delta t) = \langle \mathbf{x}_i(t) \cdot \mathbf{x}_i(t + \Delta t) \rangle \,, \tag{5.5}$$

where $\mathbf{x}_i$ can be replaced by either the directional vector or the velocity vector. It is important to note that the absence of a smooth correlation function is likely due to limited resolution, and caution should be exercised when interpreting these results. Higher-resolution calculations would be required to properly observe the decay and determine the relevant timescale.

5.5 Conclusions

A computational model was developed that successfully models the adsorption of dimers in the presence of affinity zones on the wall. The system exhibits an emergent orientation of the dimers, resulting from effective particle interactions and pressure effects. Furthermore, the

model captures the behavior of dimers transiently moving along the wall. A competition in dimer adsorption was observed, driven by the heterogeneity of the wall surfaces.

Chapter 6

Dynamic Case

6.1 Abstract

As discussed throughout this project, the bacteria targeted by phages are motile, such motility stress the fluid around it, and hydrodynamic effects may influence the adsorption of virus. Therefore, it is necessary to incorporate bacterial motility in some form, in this case, by introducing flow into the system. The flows considered are those described in section 4.3, namely Couette and Poiseuille flows. The effect of these flows on the adsorption dynamics was analyzed, and the results were fitted to adsorption models.

6.2 Non-Slip Conditions

To introduce a flow, such as Poiseuille flow, it is necessary to apply a pressure gradient. Additionally, as discussed in Section 4.3, it is essential to implement non-slip boundary conditions. In the context of computational simulations, this could be achieved by using rough walls. The presence of rough walls induces interactions that slow down the particles near the boundaries. A snapshot of the simulation box with rough walls is shown for illustration in figure 6.1.

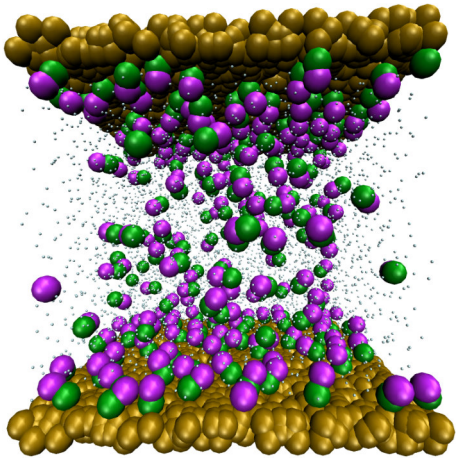

Figure 6.1: Snapshot of the simulation box with rough walls.

The system is identical to the static case, consisting of 1500 particles per wall and a wall-to-wall distance of 10, but with the presence of roughness in this flow configuration. The roughness was generated as follows: the wall was composed of three layers, and in each layer particles were placed at random positions within the plane of the layer. At this point, we consider two distinct systems: a smooth configuration with slip boundary conditions and a rough configuration with no-slip boundary conditions.

6.3 Poiseuille With Non-Slip Conditions

Simulations were developed by applying a pressure gradient to the fluid. That is, in addition to the DPD forces, a constant external force was added in the x-direction. Section 4.3.3 presents the resulting velocity profiles of the fluid. In this section, dimers were introduced into the simulation box, and adsorption isotherms were computed for different values of the applied force.

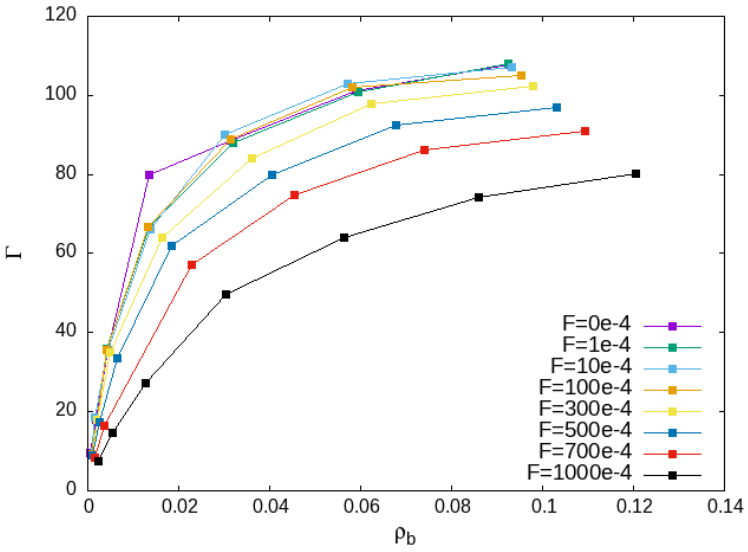

Figure 6.2: Plot of adsorption isotherms with a Poiseuille flow. Rough walls and different values for the constant external force.

In figure 6.2, the equation (5.1) is used. It can be observed that for low external forces, the adsorption remains unchanged. However, once the force exceeds 10^{-2}, as the force increases, the maximum adsorption begins to decrease consistently. This indicates that the flow affects the adsorption capacity of the dimers. We can fit the adsorption curves to the Langmuir model, expressed as follows

$$\Gamma_L = \Gamma_{max} \frac{K\rho_b}{1 + K\rho_b}, \tag{6.1}$$

where Γ_{max} is the maximum adsorption capacity and K is an adsorption constant. In figure 6.3 you can observe the fitting using Langmuir model.

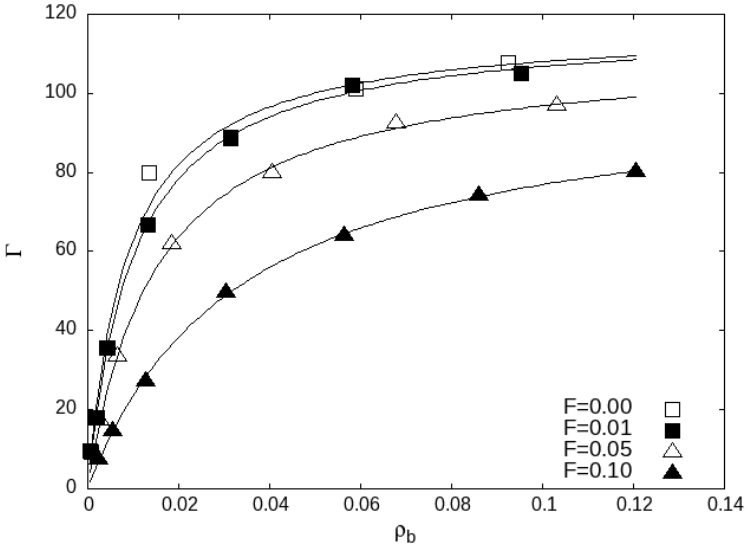

Figure 6.3: Plot of adsorption isotherms with a Poiseuille flow. Rough walls and some different values for the constant external force. The solid line is a Langmuir fit.

6.4 Poiseuille With Slip Conditions

Based on the results for Poiseuille flow with rough walls, it is natural to investigate whether a similar behavior would arise with smooth walls, thereby evaluating the influence of slip boundary conditions on adsorption.

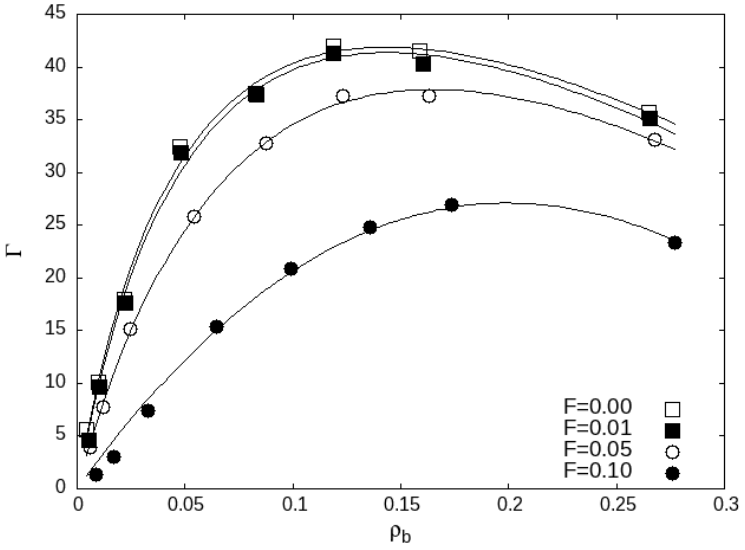

Figure 6.4: Plot of adsorption isotherms with a Poiseuille flow. Smooth walls and some different values for the constant external force. The solid line is a fit like section 5.4.

Figure 6.4 shows that, similarly, the maximum adsorption peak decreases as the flow intensity increases. However, an interesting phenomenon emerges: the number of adsorption events is almost half of that observed under no-slip conditions. In figure 6.3, adsorption values reach up to 100 on the y-axis, whereas in figure 6.4 they only reach about 40. Another noteworthy result is that, in this case, the adsorption peak occurs at higher bulk concentrations compared to the no-slip condition.

6.5 Couette With Non-Slip Conditions

We also conducted simulations under Couette flow, by assigning a positive velocity to the upper wall and an equal but opposite velocity to the lower wall. A systematic set of tests was performed for different wall velocities, and the adsorption isotherms were analyzed analogously to

the Poiseuille flow case.

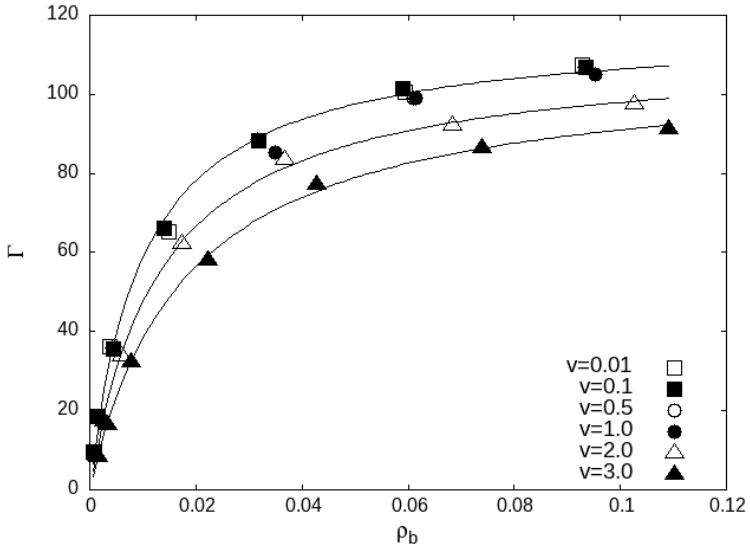

Figure 6.5: Plot of adsorption isotherms with a Couette flow. Rough walls and different values for the constant velocity of the walls. The solid line is a Langmuir fit.

As in the Poiseuille case, no significant changes in the adsorption isotherm are observed at low velocities in figure 6.5. However, once the velocities exceed the order of 10^0, the maximum adsorption progressively decreases with increasing velocity.

Chapter 7

Conclusions and Perspectives

The dimers system was successfully characterized using extensive data obtained from mesoscopic computational simulations. The effect of hydrophobicity was analyzed independently to assess its influence on the density profiles. Adsorption was also studied in the presence of heterogeneous walls. A significant impact of wall heterogeneity was observed, both on the measured observables and on the adsorption dynamics. A competition in adsorption between dimers was observed due to the heterogeneity introduced in their repulsive interaction parameters, which was an unexpected result.

Regarding the alignment results, our analysis indicates that the polar order undergoes a transition as surface affinity increases, marking the point at which thermal fluctuations no longer dominate the system's behavior. This suggests that higher affinity regions promote orientational stability among the dimers. Similarly, the wall-order parameter exhibits a clear transition between distinct regimes, further confirming the strong dependence of orientational organization on the spatial distribution of affinity zones.

For the motility case (non-zero flow), to model Poiseuille and Cou-

ette flow it is necessary to add friction to the surface. One way to do this, is modify the wall rhougness to the wall. The influence of flow on dimer adsorption was characterized, showing that high flows are required to significantly affect the adsorption process

As perspectives, we need to carry out more computational simulations to better understand the transition from heterogeneous to homogeneous walls in the mean adsorption time plot.

This work has opened several lines of future research. One such direction is to continue studying the effect of chain length on the adsorption dynamics, as demonstrated in the benchmarking section of this study. This topic is of particular interest in the field of polymer physics. Other types of phages could also be studied by modifying the chain structure, since, based on the present results, such variations would undoubtedly influence the adsorption process. Another possible direction for future research lies in the structure of the wall. In this study, a square arrangement was used; however, alternative configurations such as hexagonal or triangular lattices could be explored. Investigating how these structural variations affect wall-fluid interactions would provide deeper insights into the system's behavior. Just as surface roughness influences adsorption, another way to indirectly modify this behavior would be to model the complete bacterium, since its curvature would very likely affect the adsorption process. This suggests that future work should incorporate bacterial curvature to achieve a more realistic representation of phage adsorption dynamics.

Regarding the case with flow, it is also possible to consider other types of flow, such as shear flow, to extract additional information such as the viscoelastic properties of the system. This would represent a rel-

evant contribution to the field of rheology.

With regard to the characterization of dimer orientation, the calculation of the nematic order parameter could have been included. This would complement the polar order and the wall order parameters, providing a more complete picture of dimer alignment.

Bibliography

[1] Frederick W Twort. An investigation on the nature of ultra-microscopic viruses. *Acta Kravsi*, 1961.

[2] MF d'Herelle. Sur un microbe invisible antagoniste des bacilles dysentériques. *Acta Kravsi*, 1961.

[3] Eugene V Koonin. The wonder world of microbial viruses. *Expert review of anti-infective therapy*, 8(10):1097–1099, 2010.

[4] André M Comeau, Graham F Hatfull, Henry M Krisch, Debbie Lindell, Nicholas H Mann, and David Prangishvili. Exploring the prokaryotic virosphere. *Research in microbiology*, 159(5):306–313, 2008.

[5] Roberto Danovaro, Cinzia Corinaldesi, Antonio Dell'Anno, Jed A Fuhrman, Jack J Middelburg, Rachel T Noble, and Curtis A Suttle. Marine viruses and global climate change. *FEMS microbiology reviews*, 35(6):993–1034, 2011.

[6] Mishell Poleth Ortiz Jacome and Fernando Alexis Gonzales Zubiate. Como deter a propagação de super bacterias? how to stop the spreading of super bacteria?

[7] Fernando L Gordillo Altamirano and Jeremy J Barr. Phage therapy in the postantibiotic era. *Clinical microbiology reviews*, 32(2):10–1128, 2019.

[8] Kevin L Joiner, Arlette Baljon, Jeremy Barr, Forest Rohwer, and Antoni Luque. Impact of bacteria motility in the encounter rates with bacteriophage in mucus. *Scientific reports*, 9(1):16427, 2019.

[9] Guijuan Hao, Annie I Chen, Ming Liu, Haijian Zhou, Marisa Egan, Xiaoman Yang, Biao Kan, Hui Wang, Mark Goulian, and Jun Zhu. Colistin resistance-mediated bacterial surface modification sensitizes phage infection. *Antimicrobial Agents and Chemotherapy*, 63(12):10–1128, 2019.

[10] PG Leiman, S Kanamaru, VV Mesyanzhinov, F Arisaka, and MG Rossmann. Structure and morphogenesis of bacteriophage t4. *Cellular and Molecular Life Sciences CMLS*, 60(11):2356–2370, 2003.

[11] Raul Martinez, Francisco Alarcon, Diego Rogel Rodriguez, Juan Luis Aragones, and Chantal Valeriani. Collective behavior of vicsek particles without and with obstacles*. *The European Physical Journal E*, 41(8):91, 2018.

[12] Diego Rogel Rodriguez, Francisco Alarcon, Raul Martinez, Jorge Ramírez, and Chantal Valeriani. Phase behaviour and dynamical features of a two-dimensional binary mixture of active/passive spherical particles. *Soft Matter*, 16(5):1162–1169, 2020.

[13] Gustavo Bueno, Hector De la Vega, Isela Regalado, and Francisco Alarcón. Impacto de la motilidad de las bacterias y su interacción con virus. una perspectiva desde la simulación computacional. *JÓVENES EN LA CIENCIA*, 16:1–15, 2022.

[14] Brian Zhou, Yinghao Wu, and Zhaoqian Su. Computational simulation of holin s105 in membrane bilayer and its dimerization through a helix-turn-helix motif. *The Journal of membrane biology*, 254(4):397–407, 2021.

[15] Robert Evans, Daan Frenkel, and Marjolein Dijkstra. From simple liquids to colloids and soft matter. *Physics Today*, 72(2):38–39, 2019.

[16] Ludwig Boltzmann. *Lectures on gas theory, tr*. 1964.

[17] RK Pathria and PAUL D Beale. Statistical mechanics. 3rd, 2011.

[18] Richard P Sear, Ignacio Pagonabarraga, and Andrew Flaus. Life at the mesoscale: the self-organised cytoplasm and nucleoplasm. *BMC biophysics*, 8(1):4, 2015.

[19] Pep Espanol and Patrick Warren. Statistical mechanics of dissipative particle dynamics. *Europhysics letters*, 30(4):191, 1995.

[20] Aidan P Thompson, H Metin Aktulga, Richard Berger, Dan S Bolintineanu, W Michael Brown, Paul S Crozier, Pieter J In't Veld, Axel Kohlmeyer, Stan G Moore, Trung Dac Nguyen, et al. Lammps-a flexible simulation tool for particle-based materials modeling at the atomic, meso, and continuum scales. *Computer physics communications*, 271:108171, 2022.

[21] Shafat Mubin, Jichen Li, and Steven Plimpton. *Extending and Modifying LAMMPS Writing Your Own Source Code: A pragmatic guide to extending LAMMPS as per custom simulation requirements*. Packt Publishing Ltd, 2021.

[22] Norman H Olson, Mari Gingery, Frederick A Eiserling, and Timothy S Baker. The structure of isometric capsids of bacteriophage t4. *Virology*, 279(2):385–391, 2001.

[23] DJ De Rosier and Aaron Klug. Reconstruction of three dimensional structures from electron micrographs. *Nature*, 217(5124):130–134, 1968.

[24] E Goldberg. Recognition attachment, and injection. *Molecular biology of bacteriophage T4*, pages 347–356, 1994.

[25] Mario E Cerritelli, Joseph S Wall, Martha N Simon, James F Conway, and Alasdair C Steven. Stoichiometry and domainal organization of the long tail-fiber of bacteriophage t4: a hinged viral adhesin. *Journal of molecular biology*, 260(5):767–780, 1996.

[26] Fumio Arisaka, Moh Lan Yap, Shuji Kanamaru, and Michael G Rossmann. Molecular assembly and structure of the bacteriophage t4 tail. *Biophysical reviews*, 8(4):385–396, 2016.

[27] Michael P Allen and Dominic J Tildesley. *Computer simulation of liquids*. Oxford university press, 2017.

[28] Max Born. *Ueber anisotrope Flüssigkeiten: Versuch einer Theorie der flüssigen Kristalle und des elektrischen Kerr-Effekts in Flüssigkeiten*. 1916.

[29] Robert D Groot and Patrick B Warren. Dissipative particle dynamics: Bridging the gap between atomistic and mesoscopic simulation. *The Journal of chemical physics*, 107(11):4423–4435, 1997.

[30] Armando Gama Goicochea and Francisco Alarcón. Solvation force induced by short range, exact dissipative particle dynamics effective surfaces on a simple fluid and on polymer brushes. *The Journal of chemical physics*, 134(1), 2011.

[31] Jacob N Israelachvili. *Intermolecular and surface forces*. Academic press, 2011.

[32] A Gama Goicochea. Adsorption and disjoining pressure isotherms of confined polymers using dissipative particle dynamics. *Langmuir*, 23(23):11656–11663, 2007.

[33] David Tong. Lectures on fluid mechanics. *Lectures given at Cambridge University*, 2022.

[34] Dmitry A Fedosov, Igor V Pivkin, and George Em Karniadakis. Velocity limit in dpd simulations of wall-bounded flows. *Journal of Computational Physics*, 227(4):2540–2559, 2008.

[35] Bo Hu, William Margolin, Ian J Molineux, and Jun Liu. Structural remodeling of bacteriophage t4 and host membranes during infection initiation. *Proceedings of the National Academy of Sciences*, 112(35):E4919–E4928, 2015.

[36] Daan Frenkel and Berend Smit. Molecular simulation: from algorithms to applications. *Florida*, 2000.

Chapter 8

Appendix

8.1 Adsorption in function of affinity zone

In this work we have varied the viral load, in contrast we can vary χ value too, this is important to see how the system is perturbated by the affinity zone size, we have the same results but different presentation.

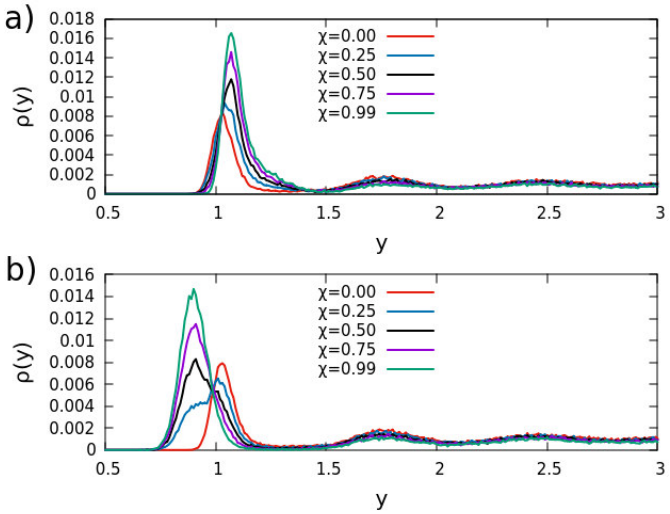

Figure 8.1: Density profile of dimers with different χ with $V_L = 160$. a) Head profiles. b) Tail profiles.

In figure 8.1b a transition is observed when χ goes from 0.00 to 0.25. There is a displacement by the peak closer to the wall, we can

caracterize this adsorption as we did previously.

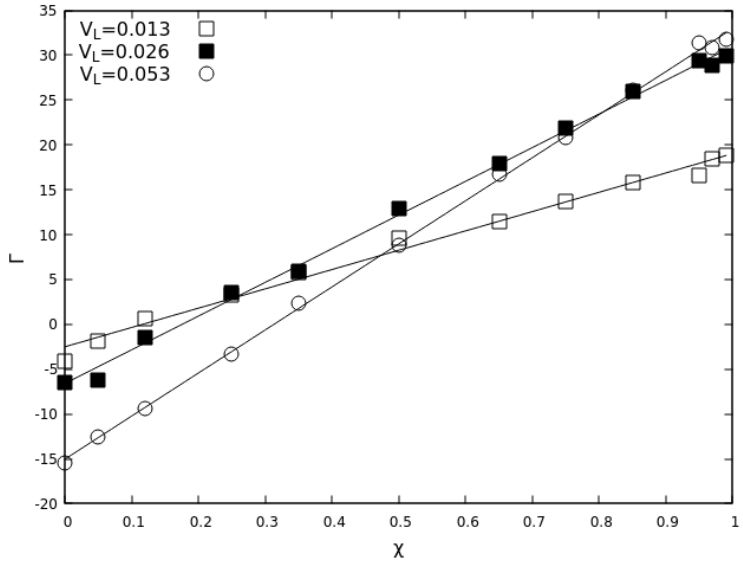

Figure 8.2: Plot of adsorption isotherms Γ with different V_L. Solid lines are linear fits.

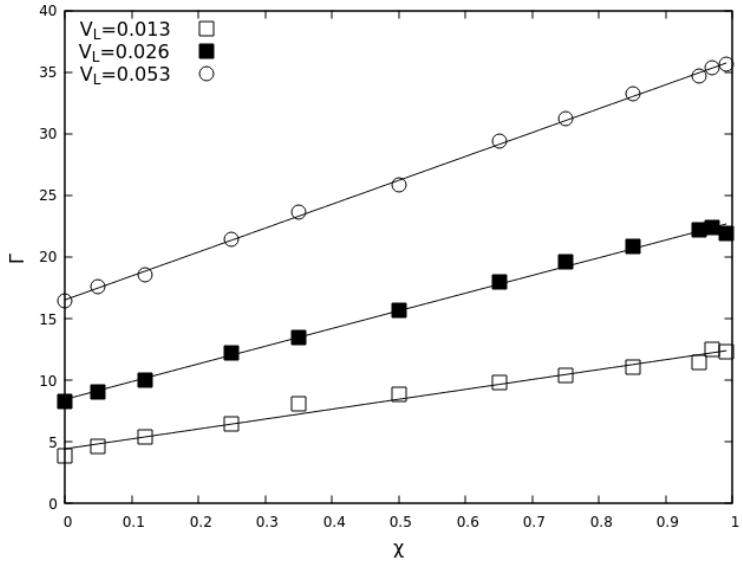

Figure 8.3: Plot of absolute adsorption isotherms Γ_{abs} with different V_L. Solid lines are linear fits.

V_L	0.013	0.026	0.053
$\frac{d\Gamma}{d\chi}$	21.5371	37.5698	48.0169
$\frac{d\Gamma_{abs}}{d\chi}$	8.03597	14.3562	19.3907

Table 8.1: Values of the rate of change for each adsorption isotherm at different viral loads.

The result obtained in figure 8.2 shows that the adsorption grows as χ increases in the 3 cases, however there is a intersection by the 3 adsorptions. For small values of χ, the adsorption increases as the viral load decreases. In contrast, for large values of χ, the adsorption increases with increasing viral load. While in figure 8.3 there is a linear increase with χ too. For both plots, the rate of change of Γ with respect to χ increases as the viral load increases, as you can see in table 8.1. This allows us to quantify how sensitive the adsorption responds to changes in wall affinity under varying system densities.

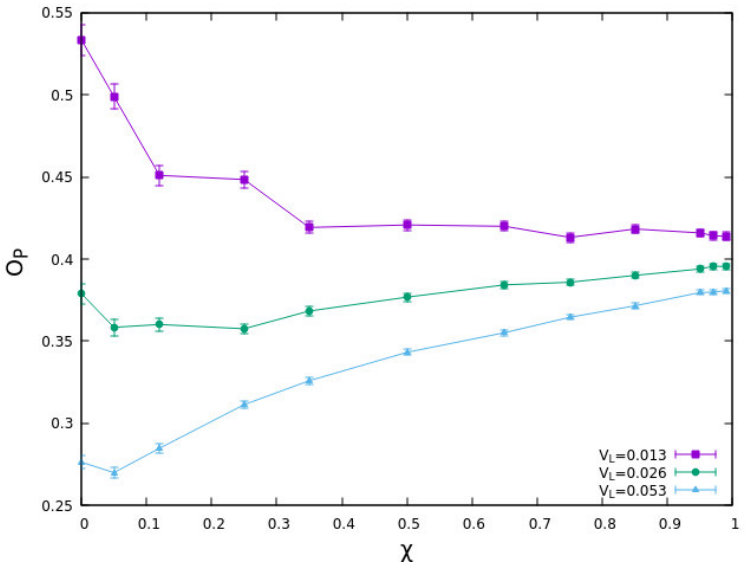

Figure 8.4: Polar-Order close to the wall with 3 values of viral load, 40, 80 and 160 virus. Varying χ in x-axis

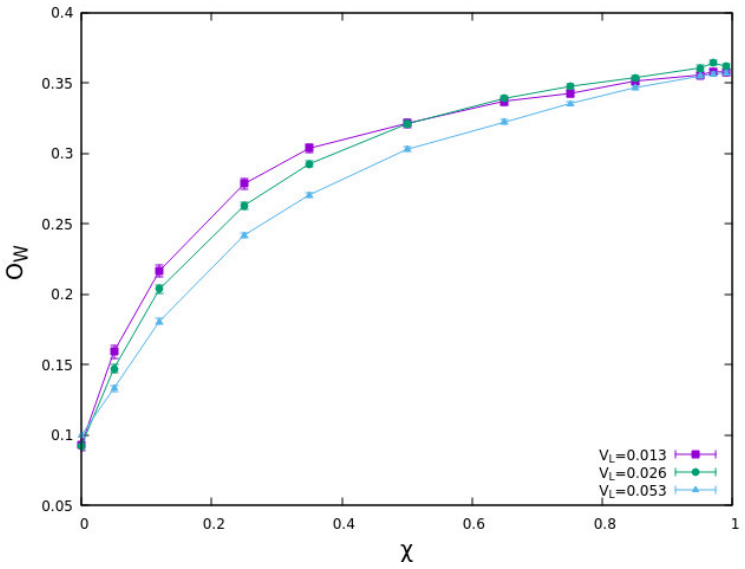

Figure 8.5: Wall-Order with 3 values of viral load, 40, 80 and 160 virus. Varying χ in x-axis

In figure 8.4, caution must be exercised when interpreting the case with $V_L = 0.013$ and $\chi = 0$, since the number of particles is very lim-

ited. It is also important to note that, for the three cases considered, the system converges to a polar order that is independent of χ. Talking about the O_W in figure 8.5 you can see the same behaviour with the 3 values of viral load showed. Increasing as the χ value increase and arriving to a O_W commun maximum value.

Universidad de Guanajuato

CAMPUS LEÓN
DIVISIÓN DE CIENCIAS E INGENIERÍAS
DEPARTAMENTO DE INGENIERÍA FÍSICA

León, Guanajuato, a 21 de enero de 2026

Dr. Modesto Sosa Aquino
Director de División DCI

Por medio de la presente le informo que he revisado el proyecto de investigación de Isael Aaron Segoviano Caudillo, estudiante del PE de Maestría en Física, con título **Computational study of phage adsorption dynamics on cell membranes**, y cumple los requisitos para poder realizar su defensa pública.

Gracias por su atención

Dr. Alejandro Gil-Villegas
Departamento de Ingeniería Física

UNIVERSIDAD DE GUANAJUATO
Campus León
División de Ciencias e Ingenierías

León, Gto., 05 de enero de 2026.

Director Dr. Modesto A. Sosa Aquino

División de Ciencias e Ingenierías

PRESENTE

Estimado Dr. Sosa Aquino:

Por medio de este conducto le informo que he leído y discutido detalladamente el trabajo de tesis **Isael Aaron Segoviano Caudillo** titulado "*Computational Study of Phage Adsorption Dynamics on Cell Membranes*", dirigido por el Dr. Francisco Alarcón Oseguera, para obtener el grado de Maestro en Física. Isael Aaron realizó un trabajo teórico-computacional mediante la técnica conocida como Dinámica de Partículas Disipativas (DPD; por sus siglas en inglés) para entender la adsorción física de bacteriófagos en paredes o superficies de bacterias. Estoy satisfecho con el contenido de la tesis, la contribución y el conocimiento obtenido y generado por Isael Aaron, por lo que no tengo inconveniente porque el trabajo sea defendido en la fecha que resulte más conveniente.

Sin otro particular por el momento, aprovecho la ocasión para enviarle un cordial saludo y quedo atento a cualquier información requerida derivada del contenido de este documento.

Atentamente,

"La Verdad Os Hará Libres"

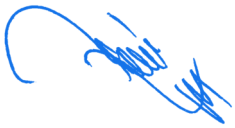

Dr. Ramón Castañeda Priego

Profesor Titular C

DEPARTAMENTO DE INGENIERÍA FÍSICA
Lomas del Bosque #103,
Lomas de Campestre, León Gto.
C.P. 37150
(477) 788 5100 Ext. 8411 y 8462
Fax. Ext. 8410
www.depif.ugto.mx

Asunto: Carta conformidad
Tesis Maestría

León, Gto., 8 de enero de 2026

Dr. Modesto Antonio Sosa Aquino
Director
División de Ciencias e Ingenierías

Estimado Dr. Sosa,

Por este conducto me permito comunicarle que, en relación con la tesis: **"Computational Study of Phage Adsorption Dynamics on Cell Membranes"**, que presenta el estudiante **Isael Aaron Segoviano Caudillo,** para obtener el grado de **Maestro en Física**, he leído detenidamente el documento, retroalimentado con sugerencias, correcciones y discutido su contenido con el estudiante.

Después de lo anterior, expreso mi conformidad con su contenido y considero que el documento posee el nivel requerido para un trabajo de investigación de maestría, por lo que apoyo que el mencionado trabajo sea defendido por la interesada cuando a ella le convenga.

Sin otro particular, aprovecho la presente para enviarle cordiales saludos.

Dra. Susana Figueroa Gerstenmaier
Profesora Titular

DEPARTAMENTO DE INGENIERÍAS QUIMICA, ELECTRONICA Y BIOMEDICA,
DIVISION DE CIENCIAS E INGENIERÍAS, CAMPUS LEÓN
Loma del Bosque 103, Fracc. Lomas del Campestre C.P. 37150 León, Gto., C.P. 37000 Tel. (477) 788-5100 ext 8416
e-mail: sfigueroa@ugto.mx, http://www.dci.ugto.mx

Vigo, España; 27 de Enero de 2026.
Asunto: Carta de aceptación de tesis de maestría

Dr. MODESTO ANTONIO SOSA AQUINO
DIRECTOR
División de Ciencias e Ingenierías, CLE

Por este conducto deseo comunicarle que he leído con detenimiento el trabajo titulado "**Computational study of phage adsorption dynamics on cell membranes**", que para obtener el grado de Maestro en Física, presenta el estudiante **Isael Aarón Segoviano Caudillo**. Después de dicha lectura y de discusiones con el estudiante relativas al mencionado trabajo, considero que el trabajo es de un nivel adecuado como tesis de maestría, dando el visto bueno como sinodal revisor del mismo.

Quedo a su disposición para cualquier aclaración que considere pertinente en relación con este escrito.

Sin otro asunto que tratar, me despido enviándole un cordial saludo.

A T E N T A M E N T E.
"LA VERDAD OS HARÁ LIBRES"

José Torres A

Dr. José Torres Arenas

DIVISIÓN DE CIENCIAS E INGENIERÍAS, CAMPUS LEÓN

Loma del Bosque 103, Fracc. Lomas del Campestre C.P. 37150 León, Gto., Ap. Postal E-143 C.P. 37000 Tel. (477) 788-5100 Fax:(477) 788-5100 ext. 8410, http://www.ifug.ugto.mx